Interactive NBI and (E)NNC methods for the progressive exploration of the criteria space in multi-objective optimization and optimal control

Mattia Vallerio[a], Dominique Vercammen[a], Jan Van Impe[a], Filip Logist[a,*]

[a] *BioTeC+ & OPTEC, Chemical Engineering Department, KU Leuven*
W. de Croylaan 46, 3001 Leuven, Belgium

Abstract

A wide range of problems arising from real world applications present multiple and conflicting objectives to be simultaneously optimized. However, this multi- objective nature is too often neglected. Multi-objective optimization proved to be a powerful tool to correctly describe the trade-offs among conflicting objectives in a set of optimal solutions known as the Pareto set. This paper introduces an interactive method to solve multi-objective problems based on geometric considerations. The method returns a wider Pareto set, at a negligible computational cost, when compared to existing methods. The interactivity also allows the decision-maker to explore only relevant parts of the Pareto set. The extreme solutions yield insightful considerations on the generation of the scalarization parameters for the Normal Boundary Intersection and the Enhanced Normalized Normal Constraints methods. The proposed method is applied to: (i) three scalar multi-objective problems, (ii) the multi-objective optimal control of a tubular and (iii) a fed-batch reactor.

Keywords: multi-objective optimization, optimal control, (Enhanced) Normalized Normal Constraint, Normal Boundary Intersection, nonlinear optimization

*Corresponding author
Email address: filip.logist@cit.kuleuven.be (Filip Logist)

1. Introduction

In recent years, due to several socio-economic reasons, profit margins for the industry have become narrower. Therefore, there is a need to operate existing processes, and design new ones, by pushing them to *extreme* operating conditions. Multi-objective optimization (MOO) enables the systematic detection of the underlying trade-offs between different objectives that should be met at the same time, e.g., minimizing energy consumption while maximizing production. Explicitly accounting for this multi-objective nature gives rise to a set of *Pareto optimal solutions* instead of a single optimum. Each Pareto point has different values for each objective function, and it is not possible to improve one objective without worsening another one. Hence, to make a selection the *decision maker* (DM) needs to provide his/her *preferences* about the investigated objective functions (Eichfelder (2008); Jahn (1984); Marler & Arora (2004); Miettinen (1999)).

Most often, the multi-objective aspect is solved by constructing a global objective function consisting of a Weighted Sum (WS) of the single objectives. The selection of weights reflecting the DM's preferences is in general non-trivial, especially when no price information is available and/or the different objective functions are incommensurable (i.e., have different units). Another well known scalarization approach is the $\epsilon-$constraint method (Haimes et al. (1971)). This method requires bounds for each objective function to be known *a priori*. The method is able to return any point on the entire Pareto set and each solution is guaranteed to be weakly Pareto optimal, however, it presents also some drawbacks: (i) it might be non-trivial to *a priori* define appropriate bounds for each objective function, (ii) it is hard to prove the uniqueness of a solution (unless problem is convex) and (iii) a uniform variation of ϵ may lead to non-uniform distribution on the Pareto set. More recently, novel scalarization approaches, such as the Normal Boundary Intersection (NBI) (Das & Dennis (1998)), (Enhanced) Normalized Normal Constraint ((E)NNC) (Messac & Mattson (2004); Sanchis et al. (2008)) and the adaptive method (Eichfelder (2009a)), based on

the Pascoletti-Serafini scalarization scheme (Pascoletti & Serafini (1984)), have been reported to mitigate these drawbacks. Additionally, it has been shown in Logist et al. (2010a, 2012) that the integration of optimal control methods with these scalarization approaches leads to an efficient solution of challenging Multi-Objective Optimal Control Problems (MOOCPs). This field of research has been particularly active in the last decade and new methods to efficiently tackle non-convex optimal control problems are currently developed (Yalçma Kaya & Maurer (2014)) and applied to different engineering fields (Alvarez-Vázquez et al. (2010)).

However, the considered scalarization methods do not always represent the complete Pareto set for problems with more than two objectives. In particular, the obtained subset typically represents only the central part of the set, leaving the *extreme* regions unexplored. The kind of information obtained by the exploration of such regions can be valuable for the DM. In particular, the *extreme* regions are at the border of the feasible set and highlight the *extreme* operating conditions.

On the contrary, evolutionary strategies (see, e.g., Deb (2001); Deb & Jain (2014)) are potentially able to cover the entire Pareto set and have been also successfully used to solve MOOCPs (Deb et al. (2004); Sarkar & Modak (2004); Agrawal et al. (2006)). The main drawbacks of these approaches still remain related to the considerable computational time required to achieve the desired solution. Recently, to compensate this drawback interactivity features have been introduced along with evolutionary strategies (see e.g., Kollat & Reed (2007); Chaudhuri & Deb (2010); Gong et al. (2014); Hettenhausen et al. (2014); Sinha et al. (2014)). However, since this work is based on deterministic scalarization based approaches, for the sake of brevity a detailed discussion on evolutionary based methods is not reported here. The interested reader is referred to, e.g, Bhaskar et al. (2000); Konak et al. (2006).

Postprint version of paper published in Comp. & Chem. Eng. 2015, vol. 82, p. 186-201.
The content is identical to the published paper, but without the final typesetting by the publisher.

Some schemes that fully describe the Pareto set for scalar multi-objective optimization problems exists. In Das & Dennis (1998) a set of additional optimizations was solved to detect the boundary of the feasible set. The number of additional problems is given by the possible pairwise combinations of objectives, hence it drastically increases with the number of considered objectives. A similar method is proposed in Motta et al. (2012), the difference being that an even distribution of the solutions on the Pareto set is guaranteed by applying a Centroidal Voronoi Tesselation algorithm (Du et al. (1999)). Kim & de Weck (2006) introduced a method that adaptively changes the set of weights of the WS to cover additional parts of the Pareto set. Then, Messac & Mattson (2004) extended the NNC method to completely cover the Pareto frontier. Here, the CHIM is first expanded to include the perpendicular projection of the hyper volume containing the entire feasible space and then it is reduced by eliminating feasible regions that are dominated by the anchor points. However, with this methodology a significant number of points yields an unfeasible NNC subproblems. Finally, Mueller-Gritschneder et al. (2009) present a successive methods to systematical cover the entire Pareto frontier, the algorithm scheme presented there closely resembles the one presented by Motta et al. (2012) where first all the boundaries or *trade-offs limits* of the Pareto set should be calculated. Once the *trade-offs limits* are obtained then the Pareto set is populated with solutions at the centre of the set. Unfortunately, the method proposed by Mueller-Gritschneder et al. (2009) also present significant computational times due to the solution of a linear programming to locate the points in the weight space. Additionally, it does not present any interactive features, hence, it also require the entire Pareto front to be investigated and can not exploit an earlier definition of preference by the DM.

Optimization and optimal control problems in general can result in numerically challenging problems. This aspect translates in quite significant computational time spent before achieving a solution. An additional complication for MOO is given from the simultaneous presence of conflicting and incommensu-

Journal homepage: http://www.journals.elsevier.com/computers-and-chemical-engineering/
Original file available at: http://www.sciencedirect.com/science/article/pii/S0098135415002355

rable objectives. Hence, in order to alleviate the computational burden and actively exploit the DM's knowledge of the treated problem several interactive MOO strategies have been developed, e.g., the interactive weighted Tchebycheff method Steuer & Choo (1983), the Light Beam Search Jaszkiewicz & Słowinski (1999) and the NIMBUS method Hakanen et al. (2005); Miettinen & Mäkelä (1995); Ojalehto et al. (2014).

In the current work an interactive method to describe an extended Pareto set is introduced. The proposed method is based on geometric considerations and presents a negligible computational effort. It is important to note that the proposed algorithm does not guarantee to find the entire Pareto set and this is ultimately not its final aim. In particular, the proposed algorithm allows to gradually extend the exploration of the Pareto set towards interesting parts for the DM. Hence, it introduces an additional degree of freedom for the DM, who can actively choose which *extreme* part of the Pareto set to investigate. In particular, after the *individual minima* cost vectors are obtained, the DM can directly explore one of the *extreme* regions without looking in the central part of the Pareto set. The method is successfully applied to both NBI and (E)NNC and it is presented here in a gradient based optimization framework which is particularly suitable for the solution of MOOCPs.

The paper is structured as follows. Section 2 introduces the formulation for MOO and reviews the WS, NBI and (E)NNC methods. Section 3 presents the extension to MOOCPs. Section 4 discusses the proposed method and the simplicial discretization of the weight space. Section 5 presents three scalar and two optimal control case studies and discusses the results. Finally, the conclusions are summarized in Section 6.

Postprint version of paper published in Comp. & Chem. Eng. 2015, vol. 82, p. 186-201.
The content is identical to the published paper, but without the final typesetting by the publisher.

2. Mathematical formulation

A general multi-objective optimization problem (MOOP) is formulated as follows:

$$\min_{\mathbf{y}\in\mathbb{R}^n} \{J_1(\mathbf{y}), J_2(\mathbf{y}), \ldots, J_{\mathrm{m}}(\mathbf{y})\} \tag{1}$$

$$\text{subject to}: \quad \mathbf{g}(\mathbf{y}) \geq \mathbf{0} \tag{2}$$

$$\mathbf{h}(\mathbf{y}) = \mathbf{0} \tag{3}$$

Here, $\mathbf{y}$ are all the optimization variables and the set of feasible solutions $\mathcal{S}$ is defined as all vectors $\mathbf{y}$ that satisfy the imposed constraints (2) and (3). The individual *objective functions* $J_{\mathrm{i}}(\mathbf{y})$ can be grouped into the *cost vector* $\mathbf{J}(\mathbf{y}) = [J_1(\mathbf{y}), J_2(\mathbf{y}), \ldots, J_{\mathrm{m}}(\mathbf{y})]^\intercal$ and map the feasible set $\mathcal{S}$ into the cost space yielding the *feasible criterion space* $\mathcal{J} = \{\mathbf{J}(\mathbf{y}) : \mathbf{y} \in \mathcal{S}\}$. As optimality criterion, the concept of *Pareto optimality* is adopted.

Definition. A point $\mathbf{y}^* \in \mathcal{S}$, is Pareto optimal if and only if there does not exist another point $\mathbf{y} \in \mathcal{S}$, such that $J_{\mathrm{i}}(\mathbf{y}) \leq J_{\mathrm{i}}(\mathbf{y}^*)$ for all i and $J_{\mathrm{i}}(\mathbf{y}) < J_{\mathrm{i}}(\mathbf{y}^*)$ for at least one objective function.

Furthermore, the following items are introduced in view of the upcoming method description, considering a minimization framework: the *minimizer* $\mathbf{y}_{\mathrm{i}}^*$ of the i-th cost function $J_{\mathrm{i}}(\mathbf{y})$, the *utopia point* $\mathbf{J}^* = [J_1^*, J_2^*, \ldots, J_{\mathrm{m}}^*]^\intercal$ which contains the minima of the individual objective functions $J_{\mathrm{i}}(\mathbf{y}_{\mathrm{i}}^*)$, the *individual minima* cost vectors or anchor points $\mathbf{J}(\mathbf{y}_{\mathrm{i}}^*)$, which are the cost vectors evaluated for the individual minimizers $\mathbf{y}_{\mathrm{i}}^*$, the *pay-off* matrix $\mathbf{\Phi}$, whose i-th column is $\mathbf{J}(\mathbf{y}_{\mathrm{i}}^*) - \mathbf{J}^*$, the *Convex Hull of Individual Minima* CHIM, CHIM_∞ and CHIM^+ which are respectively defined as follows.

Definition. Given the *utopia point* $\mathbf{J}^*$ and the individual minima cost vectors $\mathbf{J}(\mathbf{y}_{\mathrm{i}}^*)$, then the set of points in $\mathbb{R}^{\mathrm{m}}$ that are a convex combination of $\mathbf{J}(\mathbf{y}_{\mathrm{i}}^*)$

Journal homepage: http://www.journals.elsevier.com/computers-and-chemical-engineering/
Original file available at: http://www.sciencedirect.com/science/article/pii/S0098135415002355

Postprint version of paper published in Comp. & Chem. Eng. 2015, vol. 82, p. 186-201.
The content is identical to the published paper, but without the final typesetting by the publisher.

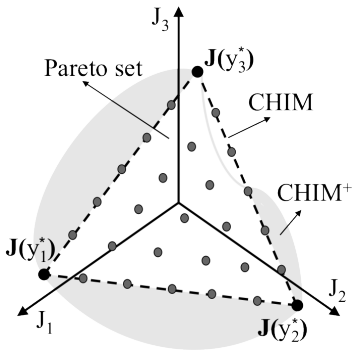

Figure 1: Schematic representation of a possible drawback arising in more than 2D problems Das & Dennis (1998). In particular the white triangle is the hyper-surface identified by the convex combination of the individual minimizers, while the grey shaded area is the projection of the feasible space in the criterion space. It is clear that some parts of the feasible space are not properly covered.

- $\mathbf{J}^*$, i.e., $\mathbf{\Phi w}$ with $\mathbf{w} \in \mathbb{R}^m, \sum_{i=1}^m w_i = 1, w_i \geq 0$, is referred to as the CHIM.

Definition. Let CHIM_∞ be the affine space of lowest dimension that contains the CHIM. Then CHIM^+ is defined as the set given by the intersection of the *feasible cost space* $\mathcal{J}$ and CHIM_∞.

Figure 1 depicts the anchor points $\mathbf{J}(\mathbf{y}_i^*)$, the Pareto set, the CHIM and the CHIM^+ for a three-objective problem. Note that the CHIM only covers the central region of the CHIM^+. As a consequence, standard scalarization methods cannot explore non-covered *extreme* regions. This paper aims to geometrically extend the CHIM in order to also explore these regions.

2.1. Scalarization methods

Scalarization methods reformulate the existing MOOP into a parametric Single Objective Optimization Problem (SOOP). By consistently varying the scalarization parameters (often called *weights* $\mathbf{w}$) an approximation of the Pareto set is obtained.

Journal homepage: http://www.journals.elsevier.com/computers-and-chemical-engineering/
Original file available at: http://www.sciencedirect.com/science/article/pii/S0098135415002355

2.1.1. Weighted Sum (WS)

The convex Weighted Sum is still often used in practice:

$$\min_{\mathbf{y}\in\mathbb{R}^n} J_{\mathrm{WS}} = \sum_{\mathrm{i}=1}^{\mathrm{m}} w_{\mathrm{i}} J_{\mathrm{i}}(\mathbf{y}) \tag{4}$$

$$\text{subject to}: \quad \mathbf{g}(\mathbf{y}) \geq \mathbf{0} \tag{5}$$

$$\mathbf{h}(\mathbf{y}) = \mathbf{0} \tag{6}$$

with $w_{\mathrm{i}} \geq 0$ and $\sum_{\mathrm{i}=1}^{\mathrm{m}} w_{\mathrm{i}} = 1$. Despite its simplicity, the WS has several intrinsic drawbacks Das & Dennis (1997). A uniform distribution of the weights does not necessarily result in an even spread on the Pareto front and points in non-convex parts of the Pareto set cannot be obtained.

2.1.2. Normal Boundary Intersection (NBI)

NBI is a specific case of the Pascoletti-Serafini method Eichfelder (2009b) and reformulates the MOOP as follows Das & Dennis (1998):

$$\max_{\mathbf{y}\in\mathbb{R}^{\mathrm{n}},\ \lambda\in\mathbb{R}} \lambda \tag{7}$$

$$\text{subject to}: \quad \mathbf{g}(\mathbf{y}) \geq \mathbf{0} \tag{8}$$

$$\mathbf{h}(\mathbf{y}) = \mathbf{0} \tag{9}$$

$$\mathbf{\Phi w} - \lambda \mathbf{\Phi e} = \mathbf{J}(\mathbf{y}) - \mathbf{J}^* \tag{10}$$

with $w_{\mathrm{i}} \geq 0$, $\sum_{\mathrm{i}=1}^{\mathrm{m}} w_{\mathrm{i}} = 1$ and $\mathbf{e} = [1, 1, ..., 1]^{\intercal} \in \mathbb{R}^{\mathrm{m}}$ the m-dimensional vector containing all ones. Hence, $\mathbf{\Phi w}$ indicates a point on the CHIM, and $-\lambda\mathbf{\Phi e}$ describes the (quasi-)normal direction to the CHIM. The rationale is that the intersection between the (quasi-)normal from any point $\mathbf{\Phi w}$ and the boundary of the feasible cost space closest to the utopia point is expected to be Pareto optimal. To this end, Eq. (7) introduces the maximization of the length λ along the (quasi-)normal described by m additional equality constraints (10). A geometric interpretation of NBI and analytic relations linking an NBI solution to the corresponding WS solution have been reported in Das & Dennis (1998).

Postprint version of paper published in Comp. & Chem. Eng. 2015, vol. 82, p. 186-201.
The content is identical to the published paper, but without the final typesetting by the publisher.

2.2. (Enhanced) Normalized Normal Constraint (E)NNC

(Enhanced) Normalized Normal Constraint reformulates the original MOOP in an alternative way:

$$\min_{\mathbf{y}\in\mathbb{R}^n} \overline{J}_m \tag{11}$$

$$\text{subject to :} \quad \mathbf{g}(\mathbf{y}) \geq \mathbf{0} \tag{12}$$

$$\mathbf{h}(\mathbf{y}) = \mathbf{0} \tag{13}$$

$$(\overline{\mathbf{J}}(\mathbf{y}^*_m) - \overline{\mathbf{J}}(\mathbf{y}^*_i))^\intercal(\overline{\mathbf{\Phi}}\mathbf{w} - \overline{\mathbf{J}}(\mathbf{y})) \geq 0 \tag{14}$$

$$\text{for } i = 1,\ldots,m-1$$

where $\overline{\ }$ indicates variables based on *normalized* objectives. The rationale is to minimize the single most important objective described by Eq. (11), while reducing the feasible cost space by adding $m-1$ hyperplanes given by Eq. (14) that are orthogonal to CHIM. Normalization is achieved by first shifting the objectives such that the utopia point coincides with the origin and afterwards pre-multiplying them with a matrix $\mathbf{T} \in \mathbb{R}^{m\times m}$:

$$\overline{\mathbf{J}}(\mathbf{y}) = \mathbf{T}(\mathbf{J}(\mathbf{y}) - \mathbf{J}^*). \tag{15}$$

Because Messac & Mattson (2004) considered only the shifting and scaling of the individual objectives in the classic NNC, the matrix $\mathbf{T}$ is diagonal with as the diagonal elements:

$$[\mathbf{T}]_{i,i} = \frac{1}{\mathbf{J}_i^{\square} - \mathbf{J}_i^*} \tag{16}$$

where $\mathbf{J}_i^{\square} = \max\{\mathbf{J}_i(\mathbf{y}^*_j), j = 1,\ldots,m\}$ is the maximum for objective function i for the set of individual minimizers $\mathbf{y}^*_j$. In their Enhanced Normalized Normal Constraint method (ENNC), Sanchis et al. (2008) introduce a different matrix $\mathbf{T}$ for a three-objective case based on the solution of a system of 9 linear equations. This matrix $\mathbf{T}$ can be generalized as follows Logist & Van Impe (2012) :

$$\mathbf{T} = \mathbf{E}\mathbf{\Phi}^{-1} \tag{17}$$

with $\mathbf{E}$ the matrix containing zeros on the diagonal and ones on the off-diagonal. As $\overline{\mathbf{\Phi}} = \mathbf{T}\mathbf{\Phi} = \mathbf{E}\mathbf{\Phi}^{-1}\mathbf{\Phi} = \mathbf{E}$. It is clear that the normalization based on Eq.

Journal homepage: http://www.journals.elsevier.com/computers-and-chemical-engineering/
Original file available at: http://www.sciencedirect.com/science/article/pii/S0098135415002355

(17) maps the individual minima to the m vertices of an m-dimensional unit hypercube. For analytic relations linking a solution of ENNC to the corresponding NBI solution, the reader is referred to Logist & Van Impe (2012).

3. Multi-Objective Optimal Control Problem

When MOO is applied to dynamic systems, Multi-Objective Optimal Control Problems are obtained:

$$\min_{\mathbf{x}(\xi),\mathbf{u}(\xi),\mathbf{p},\xi_\mathrm{f}} \{J_1,\ldots,J_\mathrm{m}\} \tag{18}$$

$$\begin{aligned}
\text{subject to :} \quad \frac{d\mathbf{x}}{d\xi} &= \mathbf{f}(\mathbf{x}(\xi),\mathbf{u}(\xi),\mathbf{p},\xi) \quad \xi\in[0,\xi_\mathrm{f}] && (19)\\
\mathbf{0} &= \mathbf{b}_\mathrm{c}(\mathbf{x}(0),\mathbf{x}(\xi_\mathrm{f}),\mathbf{p}) && (20)\\
\mathbf{0} &\geq \mathbf{c}_\mathrm{p}(\mathbf{x}(\xi),\mathbf{u}(\xi),\mathbf{p},\xi) && (21)\\
\mathbf{0} &\geq \mathbf{c}_\mathrm{t}(\mathbf{x}(\xi_\mathrm{f}),\mathbf{u}(\xi_\mathrm{f}),\mathbf{p},\xi_\mathrm{f}) && (22)
\end{aligned}$$

Here, $\mathbf{x}$ are the state variables, while $\mathbf{u}$ and $\mathbf{p}$ denote the time-varying and time-constant control variables, respectively. The vector $\mathbf{f}$ represents the dynamic system equations (on the interval $\xi\in[0,\xi_\mathrm{f}]$) with initial and terminal boundary conditions given by the vector $\mathbf{b}_\mathrm{c}$. In particular $\mathbf{f}$ can be alternatively composed by Ordinary Differential Equations (ODE), Differential Algebraic Equations (DAE) as well as Partial Differential Equations (PDE). The vectors $\mathbf{c}_\mathrm{p}$ and $\mathbf{c}_\mathrm{t}$ indicate, respectively, path and terminal inequality constraints on the states and controls. Each individual objective function can consist of both Mayer and Lagrange terms:

$$J_\mathrm{i} = h_\mathrm{i}(\mathbf{x}(\xi_\mathrm{f}),\mathbf{p},\xi_\mathrm{f}) + \int_0^{\xi_\mathrm{f}} g_\mathrm{i}(\mathbf{x}(\xi),\mathbf{u}(\xi),\mathbf{p},\xi)d\xi \tag{23}$$

Most often MOOCPs are reformulated as a WS of m objectives, e.g., in (Nonlinear) Model Predictive Control (N)MPC Vallerio et al. (2014). However, the solution of those problems with a systematic variation of weights for the WS often yields a poor representation of the Pareto set Das & Dennis (1998). In recent

years Logist et al. (2010a, 2011, 2010b, 2012) successfully combined *direct* optimal control methods such as orthogonal collocation Biegler (1984, 2007), single and multiple shooting Bock & Plitt (1984),Leineweber et al. (2003) with MOO methods such as NBI and (E)NNC to efficiently solve MOOCPs. However, in each SOOP subproblem a large-scale nonlinear optimization problem has to be solved. In particular, it was possible to achieve a better representation of the Pareto set, compared to the WS, while significantly improving the efficiency of the solution.

4. Geometric Extension of the Pareto set

Existing techniques as NBI and (E)NNC may overlook the *extreme* parts of the Pareto set. Hence, the aim of the current work is to introduce an interactive method to expand the area of the Pareto set explored by these methods. The proposed Interactive Geometric Extension (IGE) technique is based on geometric considerations and is appealing because of the low computational effort required and its interactive nature.

4.1. Central idea

The proposed procedure looks for points outside the CHIM but still belonging to the CHIM_{∞} in order to expand the scalarization parameter space and, hence, the explored criterion space. To this end, m hyperplanes are defined, such that their intersection yields a point in $\mathbb{R}^{\text{m}}$. It has to be noted that necessary conditions for the use of the proposed procedure are the existence of the individual minima and that the objectives should be bounded from below on the feasible set. In linear algebra the intersection between different elements can be represented as the solution of a system of m linear equations. The points found by plane intersections will be referred to as *external* points and they are indicated with $\mathbf{P}_*$. An *external* point is reported in Figure 2 with a grey star. These points allow to describe a first set of approximated extreme regions. However, since there is no guarantee that the *external* points will be

inside the feasible space $\mathcal{J}$, for each of them an *outer approximation* is carried out. This step aims at finding the boundaries of the CHIM$^+$. In particular, during the *outer approximation* an optimization problem is solved to deliver a feasible point on the boundary of the feasible set. The points obtained from the *outer approximation step* will be labeled as *outer* points and identified with $\mathbf{O}_*$ (see the white star in Figure 2). The space spanned by connecting the anchor points and the *outer* points is defined as CHIMO (i.e., the Convex Hull of the Individual Minima and the *Outer* points) and it approximates the CHIM$^+$.

Finally, it will be illustrated how the majority of points in the *extreme* part of the Pareto set cannot be obtained unless areas outside the CHIM$^+$ are included as well. Hence, in order to deliver a more complete representation of the Pareto front a *backtracking* line search procedure is carried out on the line segments that link each *external* point $\mathbf{P}_*$ to the respective *outer* point $\mathbf{O}_*$. In particular, the *backtracking* line search delivers the furthest points from the CHIM that still constitute feasible SOOPs and deliver Pareto candidate solutions. The points found with the *backtracking* line search procedure will be named *horizon*[1] points $\mathbf{H}_*$. A schematic representation of the proposed procedure for a three-objective problem is reported in Figure 2. Each *horizon* point $\mathbf{H}_*$ will be used as a vertex to construct m additional $(\mathrm{m}-1)$-simplices each corresponding to an *extreme* region. The collection of the additional m simplices constructed with the *horizon* points and the CHIM simplex constitutes the Convex Hull of Individual Minima and Horizon points (CHIMH). An even distribution of points on the CHIMH will give rise to a series of SOOPS problems that can be solved with the MOO method of choice, i.e., NBI or (E)NNC. The solution of the resulting set of subproblems will lead to the exploration of the *extreme* regions and, hence, to a wider representation of the Pareto front.

[1]Named after the event horizon point according to layman's terms, where it is defined as "the point of no return", i.e., the point at which the gravitational pull becomes so great as to make an escape impossible.

Postprint version of paper published in Comp. & Chem. Eng. 2015, vol. 82, p. 186-201.
The content is identical to the published paper, but without the final typesetting by the publisher.

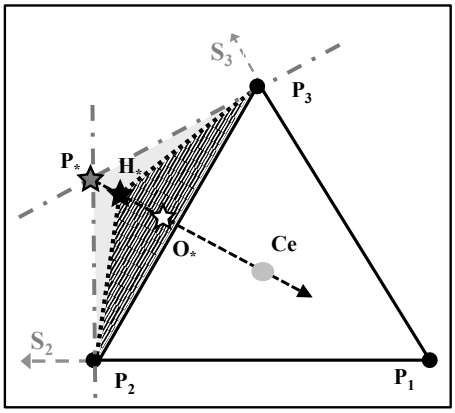

Figure 2: Geometric interpretation of the proposed technique for a 3D case. All the arising 3D geometric elements are present as 2D projections on to the CHIM_∞ plane.

4.2. Detection of the External point $\mathbf{P}_*$

The first step then consists in finding the *individual minima* cost vectors $\mathbf{J}(\mathbf{y}_i^*)$. These vectors represent m points in the $\mathbb{R}^m$ criterion space and they are going to be used to define the m linear equations needed: (i) the equation representing the hyperplane CHIM_∞ (see Section 4.2.1) and (ii) $m-1$ equations describing $m-1$ hyperplanes perpendicular to the hyperplane CHIM_∞ and normal to the *normal direction vectors* defined in Section 4.2.2. A pseudo algorithm of this procedure is reported in Algorithm 1.

4.2.1. Constructing the CHIM_∞ *hyperplane*

It is possible to obtain the equation of the hyperplane CHIM_∞ in the $\mathbb{R}^m$ objective space through the m anchor points. The general equation for a hyperplane in $\mathbb{R}^m$ can be found by constructing an $m+1$ by $m+1$ matrix and imposing its determinant to be equal to zero. For the sake of brevity, the anchor points are identified as the vectors $\mathbf{P}_i = [a_i, b_i, \cdots, m_i]^\intercal = \mathbf{J}(\mathbf{y}_i^*)$ for $i = 1, 2, \ldots, m$. Let $\mathbf{P}_* = [a_*, b_*, \cdots, m_*]^\intercal$ be the point on the hyperplane that has to be found with this procedure, then the vectors $\mathbf{P}_*$ and $\mathbf{P}_i$ can be combined to form the

Journal homepage: http://www.journals.elsevier.com/computers-and-chemical-engineering/
Original file available at: http://www.sciencedirect.com/science/article/pii/S0098135415002355

Postprint version of paper published in Comp. & Chem. Eng. 2015, vol. 82, p. 186-201.
The content is identical to the published paper, but without the final typesetting by the publisher.

Algorithm 1 Detection of the *External* point $\mathbf{P}_*$

for $i = 1 \rightarrow m$ **do**
    Find all anchor points P_i
    Define the CHIM hyperplane Eq.(25)
    Define the CHIM-simplex internal angles
procedure FIND POINT EXTERNAL TO THE CHIM:(P_*)
    Select an anchor point P_j
    for $i = 1 \rightarrow m$ **do**
        if $P_i \neq P_j$ **then**
            if Angle with vertex P_i is obtuse **then**
                Find the i-th *normal direction* as $P_i - P_{i+1}$
            else
                Find the i-th *normal direction* as in Eq.(27)
    Solve the arising linear system Eq.(29) to find the
    external point $\mathbf{P}_*$
    return $\mathbf{P}_*$

Journal homepage: http://www.journals.elsevier.com/computers-and-chemical-engineering/
Original file available at: http://www.sciencedirect.com/science/article/pii/S0098135415002355

Postprint version of paper published in Comp. & Chem. Eng. 2015, vol. 82, p. 186-201.
The content is identical to the published paper, but without the final typesetting by the publisher.

matrix:

$$\mathbf{M} = \begin{pmatrix} a_* & b_* & \cdots & m_* & 1 \\ a_1 & b_1 & \cdots & m_1 & 1 \\ a_2 & b_2 & \cdots & m_2 & 1 \\ \vdots & \vdots & \ddots & \vdots & \vdots \\ a_m & b_m & \cdots & m_m & 1 \end{pmatrix}. \tag{24}$$

To obtain the equation of the hyperplane CHIM_∞ as a function of $\mathbf{P}_*$ it is necessary to impose the determinant of the matrix $\mathbf{M}$ to be equal to zero. The above matrix represents a system of linear equations. Hence, its determinant can be calculated by applying Cramer's rule:

$$a_* C_{1,1} + b_* C_{1,2} + \cdots + m_* C_{1,m} + 1 \cdot C_{1,m+1} = 0 \tag{25}$$

in which $C_{i,j}$ are scalars called *cofactors* of the matrix $\mathbf{M}$ and are defined as:

$$C_{i,j} = (-1)^{i+j} L_j \text{ for } i = 1 \text{ and } j = 1, 2, \ldots, m \tag{26}$$

where the indices i and j indicate the position of the element of the matrix $\mathbf{M}$ whose cofactor is $C_{i,j}$. In this case, the i-th indices are fixed to 1. Additionally, $L_j, \ldots, L_m$ are the *minors* of the matrix $\mathbf{M}$, i.e., the determinants of the m by m matrices resulting by removing the first row of unknowns and the j-th column. The resulting Eq. (25) represents the hyperplane that passes through the m *individual minima* cost vectors as a function of the unknown point $\mathbf{P}_*$, i.e., the CHIM_∞. By definition, the CHIM is part of it. Figure 2 depicts the CHIM, and the CHIM_∞ as the white triangle with vertices $\mathbf{P}_1$, $\mathbf{P}_2$ and $\mathbf{P}_3$. Note that $\mathbf{P}_*$ is a coplanar point of $\mathbf{P}_1$, $\mathbf{P}_2$ and $\mathbf{P}_3$.

4.2.2. Constructing the $m-1$ *hyperplanes normal to* CHIM_∞

The definition of the additional $m-1$ hyperplanes determines in which part of the CHIM_∞ the *external* point will be positioned. In particular, there are two aspects that influence the position of the resulting point: (i) which vertex of the simplex is selected and (ii) the presence of any obtuse angle in the considered

Journal homepage: http://www.journals.elsevier.com/computers-and-chemical-engineering/
Original file available at: http://www.sciencedirect.com/science/article/pii/S0098135415002355

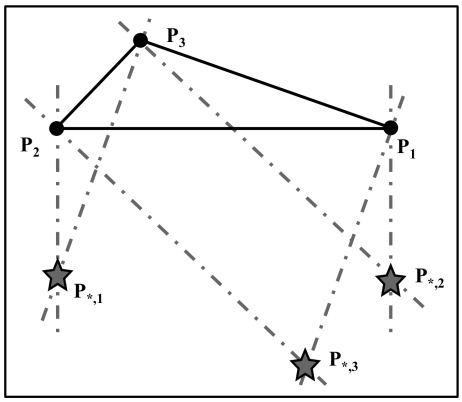

Figure 3: Geometric interpretation of the proposed technique for a 3D case when the presence of an obtuse angle is not correctly detected. All the arising 3D geometric elements are present as 2D projections on to the CHIM_∞ plane.

$(m-1)$-simplex. The selection of the vertex gives rise to the interactive nature of the proposed procedure. In fact, through this choice the DM can actively dictate the extension direction and highlight only the interesting *extreme* part of the Pareto front according to his/her preferences. From now on, whenever an angle is mentioned it is implicitly assumed that it is a 2D angle formed between two lines on the same plane, unless clearly stated.

The presence of an obtuse angle in the analyzed $(m-1)$-simplex is not relevant if the ENNC method is adopted. This is because the scaling and rotation applied to the anchors points systematically maps them to the vertex of a unit hypercube as presented by Logist & Van Impe (2012). The number of angles in an n-simplex is given by the number of 2-simplices that appear in the $(m-1)$-simplex multiplied by three, while the minimum number of angles that must be evaluated is given by the number of 2-simplices multiplied by two. Each angle is calculated via the cross product of the two vectors that generate it.

First, the procedure for problems *without obtuse angles* is presented and afterwards the necessary adjustments are introduced in case an obtuse angle is

Postprint version of paper published in Comp. & Chem. Eng. 2015, vol. 82, p. 186-201.
The content is identical to the published paper, but without the final typesetting by the publisher.

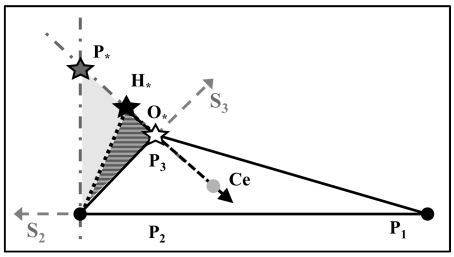

Figure 4: Geometric interpretation of the proposed technique for a 3D case in the case an obtuse angle is detected in the simplex. All the arising 3D geometric elements are present as 2D projections on to the CHIM_∞ plane.

detected. To obtain the vectors needed, one of the m *individual minima* cost vectors is selected. The $\mathrm{m}-1$ direction vectors are obtained by subtracting the selected vector from each of the remaining ones. Given $\mathbf{P}_1$, $\mathbf{P}_2$, ..., $\mathbf{P}_\mathrm{m}$ as above, the $\mathrm{m}-1$ *normal direction vectors*, in case $\mathbf{P}_1$ is selected, can be written as:

$$\mathbf{S}_\mathrm{i} = \mathbf{P}_\mathrm{i} - \mathbf{P}_1, \text{ for } \mathrm{i} = 2, 3, \ldots, \mathrm{m} \tag{27}$$

where each *normal direction vector* $\mathbf{S}_\mathrm{i}$ is a vector of the form $\mathbf{S}_\mathrm{i} = [s_{\mathrm{i},1}, s_{\mathrm{i},2}, \ldots, s_{\mathrm{i,m}}]^\intercal$. Hence, the $\mathrm{m}-1$ equations of hyperplanes with $\mathbf{S}_\mathrm{i}$ as normal vectors are:

$$\begin{aligned} &s_{\mathrm{i},1}(\mathrm{a}_* - \mathrm{a}_\mathrm{i}) + s_{\mathrm{i},2}(\mathrm{b}_* - \mathrm{b}_\mathrm{i}) \cdots + s_{\mathrm{i,m}}(\mathrm{m}_* - \mathrm{m}_\mathrm{i}) = 0, \\ &\text{for } \mathrm{i} = 2, 3, \ldots, \mathrm{m}, \end{aligned} \tag{28}$$

A particular property of all hyperplanes formed in this way is that each of them is normal to the hyperplane CHIM_∞ (that includes the CHIM). This stems from the fact that all the vectors $\mathbf{S}_\mathrm{i}$ belong to the hyperplane CHIM_∞. Figure 2 reports the constructed *normal direction vectors* $\mathbf{S}_2$ and $\mathbf{S}_3$ as gray dashed arrows. Additionally, the intersection of the CHIM_∞ with the planes identified by $\mathbf{S}_2$ and $\mathbf{S}_3$ are represented as grey dashed dotted lines that connect $\mathbf{P}_*$ to $\mathbf{P}_2$ and $\mathbf{P}_3$.

In case an *obtuse angle is detected*, it is necessary to use different $\mathrm{m}-1$ direction vectors then the ones constructed with the standard procedure. Otherwise

all *external* points will be obtained in the same *extreme* region of the CHIM_∞ (see Figure 3), resulting only in a possible partial exploration of the criterion space. To avoid this situation, the $\text{m}-1$ *normal direction vectors* have to be constructed differently. In particular, the $\text{m}-2$ generating from the vertex of the obtuse angle are constructed without using the selected vertex. A correct detection of the presence of obtuse angles is crucial to the success of the procedure. Figure 4 graphically represents the evolution of the IGE when an obtuse angle is detected. In particular, in the case depicted the selected vertex for the procedure was $\mathbf{P}_1$ and an *obtuse angle* was detected at vertex $\mathbf{P}_3$. Hence, the $\text{m}-1$ *normal direction vectors* are built as $\mathbf{S}_2 = \mathbf{P}_2 - \mathbf{P}_1$ and $\mathbf{S}_3 = \mathbf{P}_3 - \mathbf{P}_2$. The resulting *normal direction vectors* found this time are again reported as dashed grey arrows in Figure 4. In line with Figure 2 also in Figure 4 the planes corresponding to each *normal direction vector* are represented by grey dashed dotted lines from $\mathbf{P}_*$ to $\mathbf{P}_2$ and $\mathbf{P}_3$.

4.2.3. The system of m *linear equations*

Combining the equation of the hyperplane CHIM_∞ with the additional $\text{m}-1$ hyperplanes constructed above enables to write the following system of m linear equations. For the sake of brevity the system is reported in compact form:

$$\begin{cases} \det(\mathbf{M}) = 0 \\ \mathbf{S}_2(\mathbf{P}_* - \mathbf{P}_2) = 0 \\ \mathbf{S}_3(\mathbf{P}_* - \mathbf{P}_3) = 0 \\ \dots \\ \mathbf{S}_\text{m}(\mathbf{P}_* - \mathbf{P}_\text{m}) = 0. \end{cases} \tag{29}$$

The system has m degrees of freedom, which are the coordinates of the point $\mathbf{P}_*$ in $\mathbb{R}^\text{m}$. The point belongs to the hyperplane CHIM_∞ and defines an approximated *extreme* region. $\mathbf{P}_*$ is reported with a grey star marker while the approximated *extreme* region is identified by the light grey area in between $\mathbf{P}_*$, $\mathbf{P}_3$ and $\mathbf{P}_2$ (see Figures 2 and 4). Repeating this procedure m times by selecting

each time a different point than $\mathbf{P}_1$ to construct the additional m − 1 hyperplanes, delivers m additional external points to the CHIM.

It has to be noted that the method is not restricted to anchor points but it can be repeated starting from any m non-collinear points in an m dimensional space. Hence, when an approximated *extreme* region is defined, it is possible to find m−1 additional regions external to it and further from the CHIM. It has to be noted that the *external* point, found with this procedure, is not guaranteed to be inside the feasible criterion space $\mathcal{J}$. To find the contour of the intersection between the CHIM_∞ hyperplane and the feasible set $\mathcal{J}$, i.e., the CHIM^+, an outer approximation step is carried out.

Algorithm 2 Detection of the *Outer* point $\mathbf{O}_*$

1: **procedure** FIND POINT ON THE CONTOUR OF THE INTERSECTION BETWEEN THE CHIM_∞ AND THE FEASIBLE CRITERION SPACE $\mathcal{J}$: ($\mathbf{O}_*$)
2: **Find** centroid **Ce** of CHIM simplex Eq.(30)
3: **Define** the *direction* vector from $\mathbf{P}_* \rightarrow$ **Ce** Eq.(27)
4: **Solve** the optimization problem Eqs.(31) − (34)
5: to find the distance t along the direction
6: defined by Eq.(34) to obtain $\mathbf{O}_*$
7: **return** $\mathbf{O}_*$

4.3. Detecting the Outer point $\mathbf{O}_*$ via Outer Approximation

This step of the procedure is based on the concept of outer approximation (OA) used in Mixed-Integer Nonlinear Programming Duran & Grossmann (1986); Fletcher & Leyffer (1994). In particular the aim of this step is to find the last feasible point that belongs to the CHIM_∞ plane in the direction of the *external* point previously found. Three elements are needed to perform this step: (i) the *external* point, (ii) the centroid of the CHIM simplex and (iii) the direction from the *external* point towards the centroid. A pseudo algorithm for this step of the procedure is reported in Algorithm 2. The centroid of a general

m-dimensional simplex is defined as:

$$\mathbf{Ce} = \frac{1}{\mathrm{m}+1}\sum_{\mathrm{i}=1}^{\mathrm{m}} \mathbf{P}_{\mathrm{i}}. \tag{30}$$

The third required item comes from the application of Eq. (27) to find the *direction* vector from the *external* point $\mathbf{P}_*$ towards the centroid $\mathbf{Ce}$. At this point it is possible to formulate an optimization problem that closely resembles the NBI formulation in order to find the feasible point with minimum distance from $\mathbf{P}_*$ in the direction of $\mathbf{Ce}$. Mathematically, the formulation can be written as:

$$\min_{\mathbf{y}\in\mathbb{R}^{\mathrm{n}},\ \mathrm{t}\in\mathbb{R}} \mathrm{t} \tag{31}$$

$$\text{subject to}: \quad \mathbf{g}(\mathbf{y}) \geq \mathbf{0} \tag{32}$$

$$\mathbf{h}(\mathbf{y}) = \mathbf{0} \tag{33}$$

$$\mathbf{P}_* + \mathrm{t}(\mathbf{Ce} - \mathbf{P}_*) = \mathbf{0} \tag{34}$$

where t is the scalar distance along the *direction* vector identified from the additional constraint (34). This additional constraint, in analogy with NBI, forces the solution to be on the required specific direction. Moreover, the feasibility of the solution is ensured by maintaining the original constraints of the investigated problem, i.e., Eqs. (32) and (33). The solution of the OA problem delivers a feasible point on the contour of the intersection between the CHIM_∞ and the feasible criterion space $\mathcal{J}$. From now on, points obtained from the OA step will be referred to as *outer* points $\mathbf{O}_*$. The *outer* point $\mathbf{O}_*$ and the OA direction are depicted in Figures 2 and 4 as a white star and a dotted black arrow that connects $\mathbf{P}_*$ to $\mathbf{Ce}$.

4.4. Detection of the Horizon $\mathbf{H}_*$ *point via backtracking line search*

Since a full representation of the Pareto front cannot be achieved by a sole parametrization of the intersection between the CHIM_∞ and the feasible criterion space $\mathcal{J}$, which was approximated by the CHIMO, an extension towards the unfeasible parts of the CHIM_∞ is required. In particular the search is executed

Algorithm 3 Detection of the *Horizon* point $\mathbf{H}_*$

procedure FIND THE LAST POINT OUTSIDE THE FEASIBLE CRITERION SPACE $\mathcal{J}$ THAT DELIVERS A PARETO CANDIDATE POINT: ($\mathbf{H}_*$)
  Define the number of points h
  Discretize the distance from $\mathbf{P}_* \rightarrow \mathbf{O}_*$ into $\mathbf{H}_\mathrm{i}$
  equidistant points according to Eq.(35)
  for $\mathrm{i} = 0 \rightarrow \mathbf{H}_\mathrm{i}$ **do**
    Define SOOP with weights $\mathbf{w}_{\mathrm{H,i}}$ according to
    MOO method of choice
    Solve the arising SOOP
    if $\mathbf{O}_*$ closer to CHIM then $\mathbf{P}_*$ **then**
      if SOOP problem is feasible **then**
        Return $\mathbf{H}_\mathrm{i}$
        break
    else
      if SOOP problem is unfeasible **then**
        Return $\mathbf{H}_{\mathrm{i}-1}$
        break
  Discretize the distance from $\mathbf{H}_\mathrm{i} \rightarrow \mathbf{H}_{\mathrm{i}-1}$ into $\mathbf{H}_\mathrm{i}$
  equidistant points according to Eq.(35)
  for $\mathrm{i} = 0 \rightarrow \mathbf{H}_\mathrm{i}$ **do**
    Define SOOP with weights $\mathbf{w}_{\mathrm{H,i}}$ according to
    MOO method of choice
    Solve arising SOOP
    if $\mathbf{O}_*$ is closer to CHIM then $\mathbf{P}_*$ **then**
      if SOOP problem is unfeasible **then**
        $\mathbf{H}_* = \mathbf{H}_{\mathrm{i}-1}$
        Return $\mathbf{H}_*$
        break
    else
      if SOOP problem is feasible **then**
        $\mathbf{H}_* = \mathbf{H}_\mathrm{i}$
        Return $\mathbf{H}_*$
        break

by implementing a sort of backtracking line search algorithm in order to find the first point on the *direction* vector defined by Eq. (34) that delivers a Pareto candidate solution using the MOO method of choice (i.e., NBI or ENNC). In particular, the distance between the *outer* point $\mathbf{O}_*$ and the *external* point $\mathbf{P}_*$ is discretized into equidistant points $\mathbf{H}_\mathrm{i}$. Additionally, all $\mathbf{H}_\mathrm{i}$ points belong to the CHIM_∞ and they can be expressed as a linear combination of the m anchor points. As a consequence, it is possible to solve a linear system to obtain a set of scalarization parameter vectors $\mathbf{w}_{\mathrm{H,i}}$, one for each of the $\mathbf{H}_\mathrm{i}$ points. Then, if h is the number of equidistant points $\mathbf{H}_\mathrm{i}$, this results in:

$$\mathbf{H}_\mathrm{i} = \mathbf{P}_* + \frac{\mathrm{i}}{\mathrm{h}-1}(\mathbf{O}_* - \mathbf{P}_*), \text{ for } \mathrm{i} = 0, 1, \ldots, \mathrm{h}-1. \tag{35}$$

In particular, all $\mathbf{H}_\mathrm{i}$ points defined above belong to the CHIM_∞. Hence, they can also be defined as a linear combination of the m anchor points. Consequently, the corresponding scalarization parameters $\mathbf{w}_{\mathrm{H,i}} \in \mathbb{R}^\mathrm{m}$ for each of the $\mathbf{H}_\mathrm{i}$ can be determined. This set of scalarization parameters is then used to solve a sequence of SOOPs starting from point $\mathbf{P}_*$ towards point $\mathbf{O}_*$ with the MOO method of choice. In particular, the procedure is implemented differently according to the relative position of $\mathbf{O}_*$ and $\mathbf{P}_*$ in respect to the CHIM. Two situations are possible: (i) $\mathbf{O}_*$ is closer to the CHIM than $\mathbf{P}_*$ or (ii) $\mathbf{P}_*$ is closer to the CHIM than $\mathbf{O}_*$. The series stops, either when the first $\mathbf{w}_{\mathrm{H,i}}$ vector in the sequence results in a feasible SOOP (situation (i)) and delivers a Pareto candidate solution or when the first $\mathbf{w}_{\mathrm{H,i}}$ vector in the sequence results in an unfeasible SOOP (situation (ii)). At this point the distance between the $\mathbf{H}_\mathrm{i}$ point corresponding to the first feasible problem and the previous one is discretized with the same number of equidistant points according to Eq. (35).

The resulting sequence of SOOPs is solved in the opposite direction until the first unfeasible problem is found (situation (i)) or until the first feasible problem is detected (situation (ii)). The backtracking algorithm stops and the last point that delivered a candidate Pareto solution is taken as the new vertex of the *extreme* region to be discretized and is called *horizon* point $\mathbf{H}_*$. The

horizon point $\mathbf{H}_*$ is reported in Figures 2 and 4 as a black star. Note that the *backtracking* line search direction coincides with the OA direction and, hence, is also represented with a black dotted arrow (see Figures 2 and 4). The *extreme* region is represented as the hatched area between $\mathbf{H}_*$, $\mathbf{P}_2$ and $\mathbf{P}_3$ (see Figures 2 and 4). Every additional *extreme* region is a $(\mathrm{m}-1)$-simplex. Finally, the additional $(\mathrm{m}-1)$-simplices are combined with the CHIM simplex to obtain the CHIMH. The discretization of the CHIMH is achieved via the simplicial discretization method highlighted here after.

4.5. Discretization of the CHIMH

The discretization of the CHIMH is first carried out by subdividing it into $(\mathrm{m}-1)$-simplices. A schematic representation of the adopted simplicial discretization is reported in Figure 5 for a 3D case. The scalarization parameter space can in any case be represented by an $\mathrm{m}-1$ dimensional space. It has to be noted that the CHIM is always represented by a $(\mathrm{m}-1)$-simplex. The approach proposed in this work extends the use of simplices to the additional regions identified on the CHIM_∞. Moreover, lower order simplices are exploited to achieve the discretization of the scalarization parameter space. In particular, if a three-objective problem is analyzed, a series of 2-simplices is used to discretize the 2D CHIMH. Every 2-simplex in the collection is then discretized into points. The approach is based on the weight generation scheme reported in Das & Dennis (1998) and extended to an m-dimensional case. The total number of points $\mathrm{p_{CHIM}}$ to be equally distributed on the CHIM can be calculated as follows:

$$\mathrm{p_{CHIM}} = \frac{(\mathrm{m}+\mathrm{p}-2)!}{(\mathrm{m}-1)!(\mathrm{p}-1)!} \tag{36}$$

The number of points in which the additional simplices are discretized is calculated according to the proportion between the hypervolume of the considered additional simplex and the CHIM. The number of points in each additional simplex is called $\mathrm{p_{ext,i}}$ for $\mathrm{i}=1,\ldots,\mathrm{m}$ yielding a total number of points on the

Postprint version of paper published in Comp. & Chem. Eng. 2015, vol. 82, p. 186-201.
The content is identical to the published paper, but without the final typesetting by the publisher.

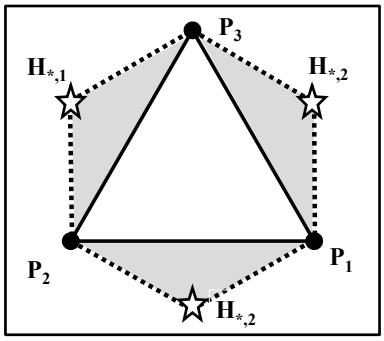

Figure 5: Simplicial discretization of the CHIMH.

CHIMH:

$$\mathrm{p_{TOT}} = \mathrm{p_{CHIM}} + \sum_{\mathrm{i}=1}^{\mathrm{m}} \mathrm{p_{ext,i}}. \tag{37}$$

5. Results and discussion

In this section the procedure is tested on three scalar Multi-Objective Optimization Problems and two Multi-Objective Optimal Control Problem.

5.1. Case I: Three-Objective Optimization Problem

The first case study has been proposed by Motta et al. (2012), and can be formulated as follows:

$$\min_{\mathbf{y}\in\mathbb{R}^3} f(\mathbf{y}) = \mathrm{y_i}, \text{ for } \mathrm{i} = 1,2,3 \tag{38}$$

subject to :

$$\begin{aligned} \mathrm{y_1} &\geq \mathrm{y_2^{-1}} + \mathrm{y_3^{-1}}, \\ \mathrm{y_2} &\geq \mathrm{y_1^{-1}} + \mathrm{y_3^{-1}}, \\ \mathrm{y_3} &\geq \mathrm{y_1^{-1}} + \mathrm{y_2^{-1}}, \\ 0.2 &\geq \mathrm{y_i} \geq 10.0, \text{ for } \mathrm{i} = 1,2,3. \end{aligned} \tag{39}$$

Journal homepage: http://www.journals.elsevier.com/computers-and-chemical-engineering/
Original file available at: http://www.sciencedirect.com/science/article/pii/S0098135415002355

The problem results in a three-objective scalar case study with three variables and nine constraints. In particular, the constraints define a very smooth but steep Pareto front. The problem serves the purpose to highlight the *extreme* zones left unexplored by the traditional NBI and ENNC methods. For this case study all the steps of the procedure are going to be covered in detail, together with the obtained numerical results.

First, the anchor points are calculated:

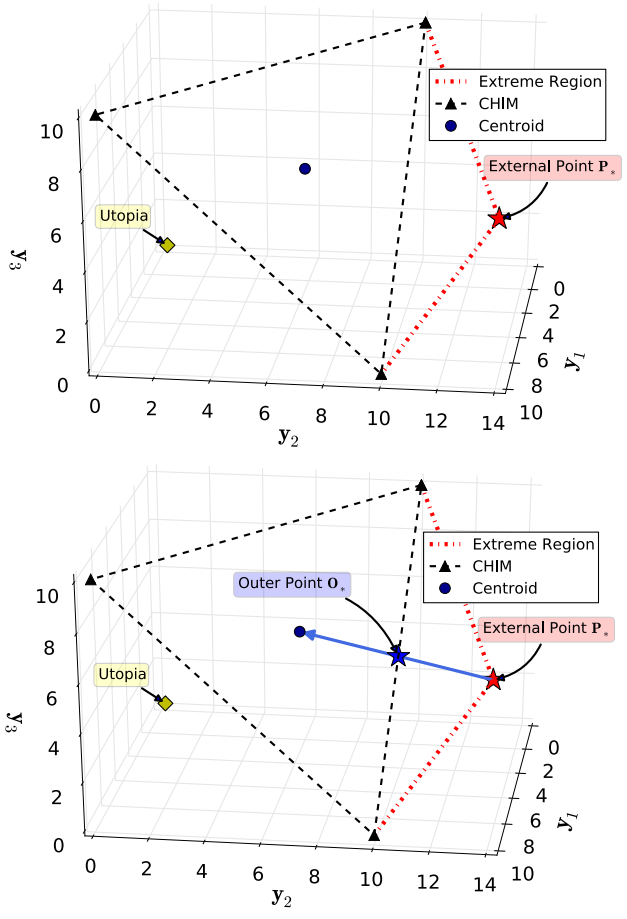

Figure 6: Detection of an *external* point $\mathbf{P}_*$ (top) and detection of an *outer* point $\mathbf{O}_*$ (bottom).

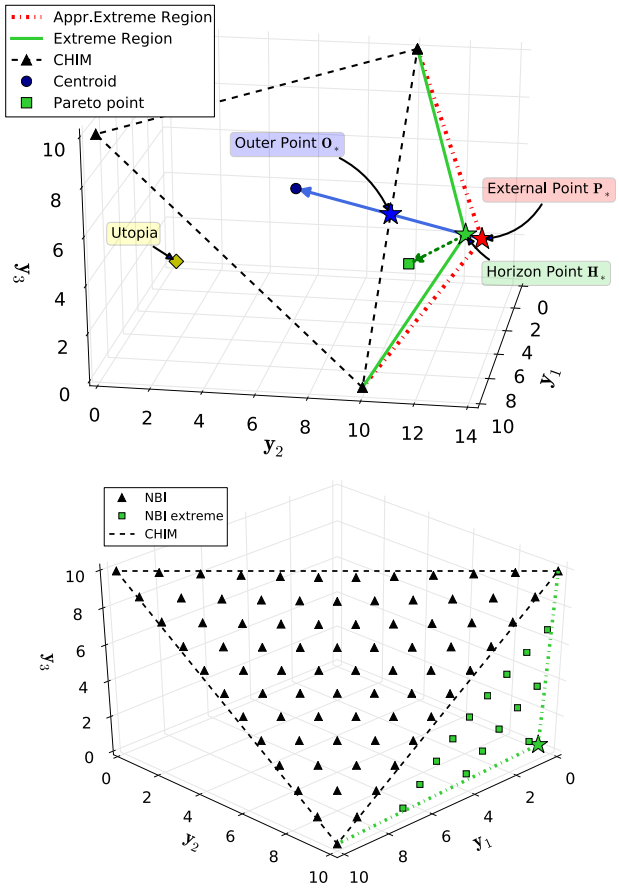

Figure 7: Detection of a *horizon* point $\mathbf{H}_*$ with resulting *extreme* region (top). The *extreme* region is then discretized into points and a SOOP is defined for each of them. The solution of the set of SOOPs with the NBI method delivers the candidate Pareto solutions which are reported as squares (bottom).

$$\begin{aligned}\mathbf{J}^*_{\mathrm{y}_1} &= [0.2 \quad 10.0 \quad 10.0]^\intercal \\ \mathbf{J}^*_{\mathrm{y}_2} &= [10.0 \quad 0.2 \quad 10.0]^\intercal \\ \mathbf{J}^*_{\mathrm{y}_3} &= [10.0 \quad 10.0 \quad 0.2]^\intercal.\end{aligned} \tag{40}$$

Once the anchor points are known, the equation of the resulting CHIM_∞ can

be calculated according to Eq. (24):

$$y_1^* + y_2^* + y_3^* - 20.2 \quad = 0.0. \tag{41}$$

In the same fashion the $(m-1)$, i.e., 2 planes perpendicular to the one represented by Eq. (41) can be calculated via Eqs. (27) and (28). If the anchor point $\mathbf{J}^*_{y_2}$ is selected the two normal planes are described by:

$$\begin{aligned} y_1^* - y_2^* + 9.8 \quad &= 0.0 \\ y_2^* - y_3^* - 9.8 \quad &= 0.0. \end{aligned} \tag{42}$$

It is possible to combine the three obtained equations into a linear system, as in Eq. (29). Its solution leads to the coordinates of the *external* point $\mathbf{P}_*$:

$$\mathbf{P}_* = [3.46 \quad 13.26 \quad 3.46]^\intercal. \tag{43}$$

The point $\mathbf{P}_*$ is reported in the top graph of Figure 6. Additionally, the three anchor points (represented by black upper triangles), the CHIM and the first approximated *extreme* region are reported. The next step is to obtain the centroid of the CHIM $\mathbf{Ce}$ with Eq. (30):

$$\mathbf{Ce} = [6.73 \quad 6.73 \quad 6.73]^\intercal. \tag{44}$$

Then the OA problem is set up as in Eqs. (31)-(34) and solved. The *outer* point $\mathbf{O}_*$ resulting from the OA step can be calculated analytically for this example:

$$\mathbf{O}_* = [5.10 \quad 10.00 \quad 5.10]^\intercal. \tag{45}$$

The point is reported in the bottom graph of Figure 6 along with the OA direction (represented by the blue arrow). Once the *outer* point is available, the *backtracking* line search is carried out along the same direction according to Algorithm 3 and Eq. (35). The *backtracking* procedure finds the *horizon* point $\mathbf{H}_*$ which is reported in the top plot of Figure 7 and has the following coordinates:

$$\mathbf{H}_* = [3.76 \quad 12.67 \quad 3.76]^\intercal. \tag{46}$$

The *horizon* point gives a feasible SOOP which is solved with the method of choice and delivers the Pareto point reported in Figure 7 as well. The arrow

from the *horizon* point $\mathbf{H}_*$ to the Pareto point represents the quasi-normal direction for the NBI method. The *horizon* point defines the *extreme* region which can then be discretized and solved with the method of choice. The bottom plot in Figure 7 depicts the *extreme* region filled with Pareto points obtained by solving additional NBI SOOPs.

The interactive nature of the proposed method has been highlighted. In fact, if the DM is satisfied with the exploration of the *extreme* region in Figure 7, the remaining part of the Pareto front can be left unexplored. Otherwise, the procedure is repeated and a more complete exploration of the criterion space is achieved (see the top graph in Figure 8). The comparison between the top and the bottom graphs in Figure 8 highlights the nature of the constructed CHIMH. A similar exploration of the criterion space can be achieved with the ENNC method.

For this case study the criterion space approximated by the CHIMH is covered with $p_{TOT} = 123$ points. The parameter p, the number of points distributed in the CHIM and in every *extreme* region are reported in Table 1. The computational time needed for the solution of the geometric extension (IGE) procedure is 0.17 s for the NBI approach and 0.07 s for the ENNC method. The total time needed to obtain the 123 Pareto optimal solutions is 0.87 s for the NBI and 1.02 s for the ENNC method (see Table 2). The Pareto fronts obtained are similar to the ones achieved by Motta et al. (2012) for the same case study.

Finally, the bottom plot of Figure 9 represents the scalarization parameter space used to realize the extended exploration of the criterion space with the NBI (see top graph in Figure 8) and ENNC. It has to be noted that the sum of scalarization parameters is still $\sum_{i=1}^{3} w_i = 1$, while now scalarization parameters are negative for points contained in the *extreme* regions. As a consequence, the last scalarization parameter omitted from the graph can be calculated by $w_3 = 1 - (w_1 + w_2)$.

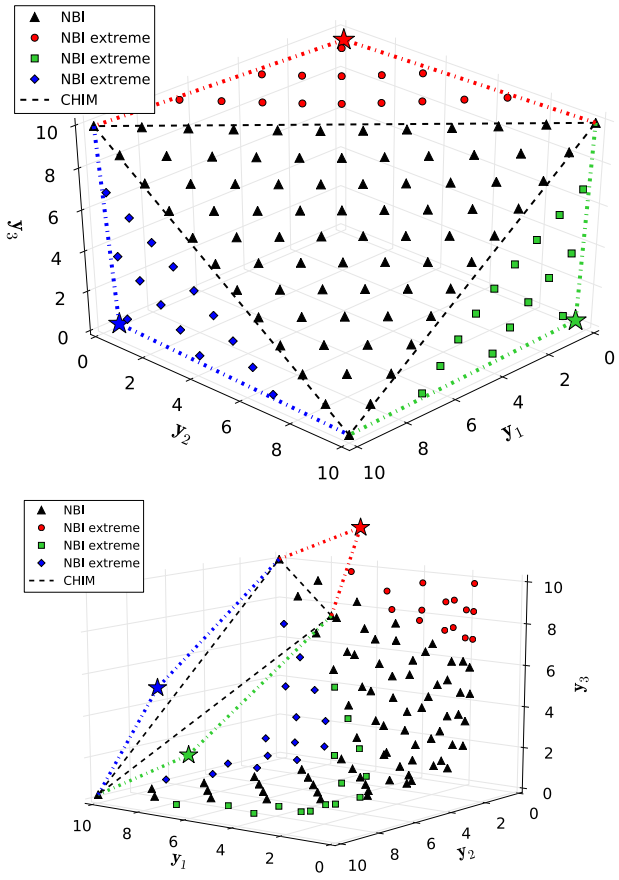

Figure 8: Isometric view (top) and skew view (bottom) of the extended criterion space explored with the NBI method.

5.2. *Case II: Four-Objective Optimization Problem*

The second case study extends the previous one by adding a fourth variable and a fourth objective to the problem formulation. As the previous case study, also this one was proposed in Motta et al. (2012) and it is formulated as follows:

$$\min_{\mathbf{y}\in\mathbb{R}^4} f(\mathbf{y}) = \mathrm{y_i}, \text{ for } \mathrm{i} = 1,2,3,4 \tag{47}$$

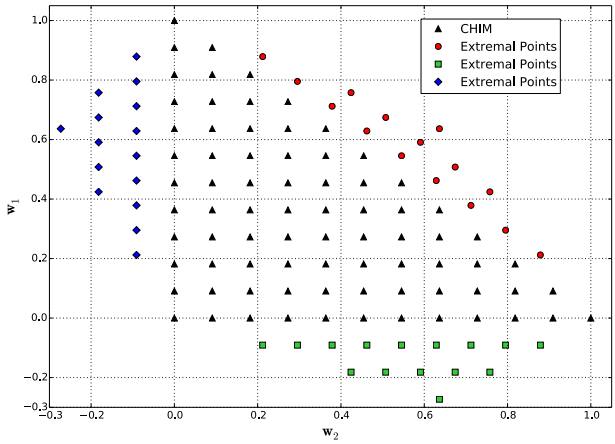

Figure 9: Representation of the scalarization parameter space that allows NBI and ENNC to explore the extended criterion space. In particular, note that $w_3 = 1 - (w_1 + w_2)$

subject to :

$$\begin{aligned} y_1 &\geq y_2^{-1} + y_3^{-1} + y_4^{-1}, \\ y_2 &\geq y_1^{-1} + y_3^{-1} + y_4^{-1}, \\ y_3 &\geq y_1^{-1} + y_2^{-1} + y_4^{-1}, \\ y_4 &\geq y_1^{-1} + y_2^{-1} + y_3^{-1}, \\ 0.2 &\geq y_i \geq 10.0, \text{ for } i = 1, 2, 3, 4. \end{aligned} \tag{48}$$

The problem is in complete analogy with the previous one and extends it to four dimensions. The problem is solved both with NBI and ENNC and its results are particularly interesting for the visualization of the simplicial discretization used. Given the higher dimensionality of the objective space the individual steps of the procedure are not visualized.

The extended criterion space found with the ENNC method is reported in Figure 10 using a total of 376 points. The parameters related to the calculation of the total number of SOOPs is reported in Table 1. It is possible to appre-

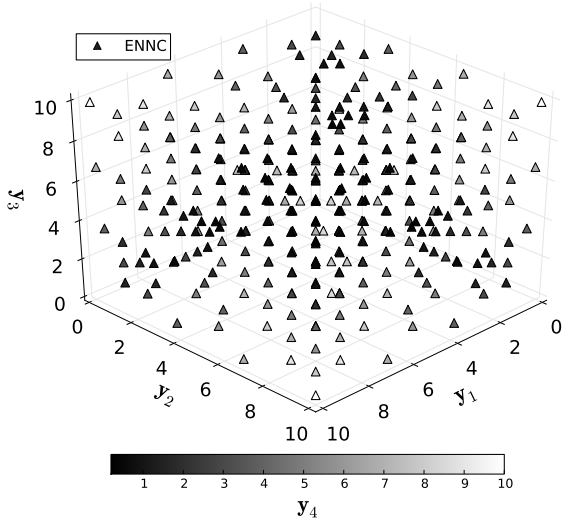

Figure 10: 4D Pareto set achieved with the ENNC method.

ciate the width of the criterion space achieved through the application of the proposed method. Due to the limitation of 3D plotting the fourth objective is rendered with the help of a progressive gradual coloration. The used color map is reported at the bottom of the plot. For this case study the computational time used for the IGE of the criterion space is 0.23 s for NBI and 0.12 s for ENNC, while the time spent for the solution of all 376 SOOPs is 2.16 s and 2.86 s for NBI and ENNC, respectively. Once again, the obtained Pareto front is similar to the one achieved by Motta et al. (2012).

The major insight gained from this case study is the visualization of the parameter scalarization space. In particular, the top graph in Figure 11 depicts the five 3-simplices that form the CHIMH for this case study. It was chosen to report only 3 scalarization parameters for each scalarization parameter vector since the fourth can be calculated as a complement to one of the sum of the other. Additionally, the geometric aspect at the base of the proposed technique is clearly visible from the top plot in Figure 11. Moreover, the simplices are then

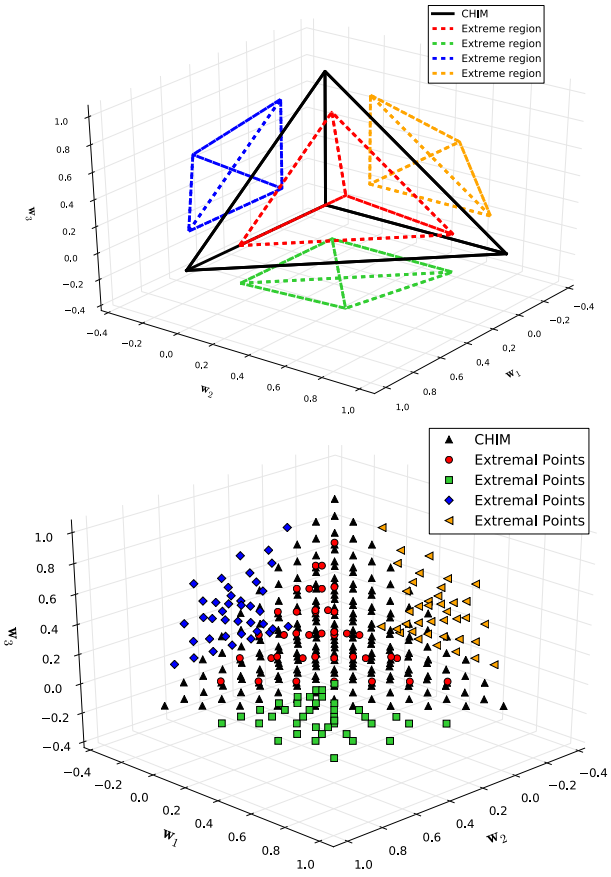

Figure 11: Simplicial discretization of the scalarization parameters space. In particular, the 5 3-simplices that define the CHIMH are depicted (top). Discretization in points of the CHIMH by evenly distribution of points in each of the 3-simplices reported in the top graph (bottom).

discretized and result in the collection of 376 points reported in the bottom plot of Figure 11.

5.3. Case III: General three-objective problem

The third example extends the two-objective example presented by, e.g., Das & Dennis (1998) by introducing an additional objective function f_3. As can be seen, this example is highly nonlinear due to the different objectives and

constraints.

$$\min_{\mathbf{y}\in\mathbb{R}^5} \begin{bmatrix} f_1(\mathbf{y}) = y_1^2 + y_2^2 + y_3^2 + y_4^2 + y_5^2 \\ f_2(\mathbf{y}) = 3y_1 + 2y_2 - \frac{y_3}{3} + 0.01(y_4 - y_5)^3 \\ f_3(\mathbf{y}) = y_1^2 + 3y_2^2 + 0.2(y_3 - y_5)^3 \\ \qquad\qquad + \log(y_4^2 + y_1^2 + y_2^2 + 1) \end{bmatrix} \tag{49}$$

$$\begin{aligned} \text{subject to :} \quad & y_1 + 2y_2 - y_3 - 0.5y_4 + y_5 - 2 = 0, \\ & 4y_1 - 2y_2 + 0.8y_3 + 0.6y_4 + 0.5y_5^2 = 0, \\ & y_1^2 + y_2^2 + y_3^2 + y_4^2 + y_5^2 \leq 10. \end{aligned} \tag{50}$$

This case study demonstrates the need to account for obtuse angles in the CHIM during the IGE procedure. When an obtuse angle is present in the CHIM and it is not correctly detected the IGE procedure finds all the m *external* points in the same region of the criterion space. In particular, all the *external* points lie in the region opposite to the vertex of the obtuse angle (see Figure 3). The top graph in Figure 12 depicts the *external* points and the approximated *extreme* regions obtained when the obtuse angle is not detected. The full lines represent two planes that internally cross the CHIM. On the contrary, a correct detection of the obtuse angle allows to find the *external* points in the desired *extreme* regions (see contrast between top and bottom graph in Figure 12). Once the *external* points are correctly detected, the IGE procedure can be completed, enabling the detection of the *outer* points and the *horizon* points for this case study. The resulting *outer* and *horizon* points are reported in Figure 13. It has to be emphasized that all geometric objects depicted in Figures 12 and 13 belong to the same plane, i.e., the CHIM_∞.

Note that, for this case only one of the *extreme* regions is detected to be outside the CHIM, while the remaining two collapse either on the edge or in the CHIM interior. This is due to the particular non-convex shape of the feasible criteria space $\mathcal{J}$. Not all points of the CHIM give rise to a feasible NBI or ENNC subproblem. Hence, only one *extreme* region will be discretized and only one additional set of SOOPs will be solved on top of the original SOOPs for the

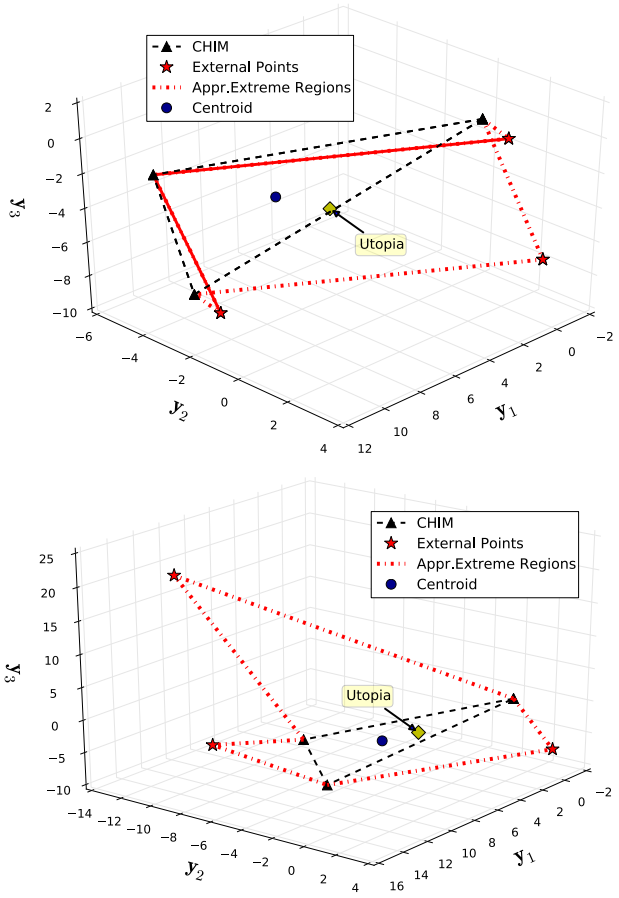

Figure 12: Detection of the *external* points when the obtuse angle is not detected (top) and when the obtuse angle is correctly detected (bottom).

CHIM. For this case study the parameter p = 11, generating 66 SOOPs inside the CHIM, while after the discretization of the *extreme* region 22 additional SOOPs are defined (see Table 1).

555

The solution of the complete set of 88 SOOPs takes 2.57 s for the NBI method. Results are depicted in the top graph of Figure 14. For the ENNC method the computational time required is 1.94 s and the achieved Pareto front is reported in the bottom graph of Figure 14. The IGE procedure is carried

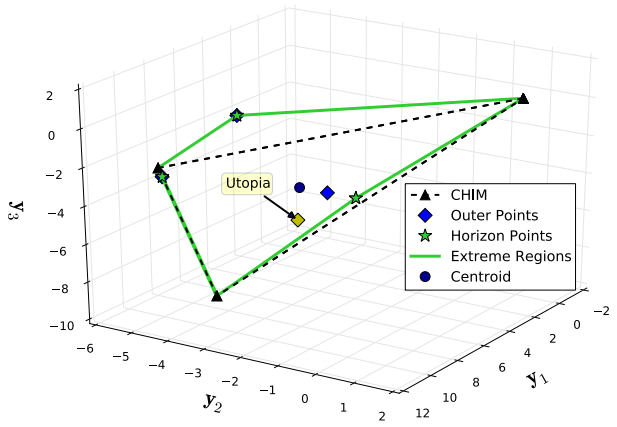

Figure 13: Construction of the *extreme* region for Case Study III. Note that only one *extreme* region extends the CHIM, while no additional Pareto candidate solution is found in the other directions.

out in 1.10 s for the ENNC and 1.73 s for the NBI method (see Table 2). It is important to notice that the significant computational time required for the IGE procedure for this problem is due to the non-convex shape of the feasible criteria space $\mathcal{J}$ and it is not directly related to the presence of an obtuse angle. Additionally, the NBI method detects 13 Pareto candidate solutions that result in dominated points and are removed after the application of a Pareto filter. This result is in line with what is reported by Logist & Van Impe (2012). The scalarization parameters used to define the 88 SOOPs are reported in Figure 15.

5.4. Case IV: Multi-Objective Optimal Control of a Tubular Reactor

In this case study a jacketed tubular reactor under steady-state conditions is considered. Inside the reactor an irreversible first-order reaction takes place. The reactor is of length L, C is the reactant concentration, T is the reactor temperature and T_{w} the jacket temperature. The mass and energy balances give rise to two coupled ODEs with the position z along the reactor as the

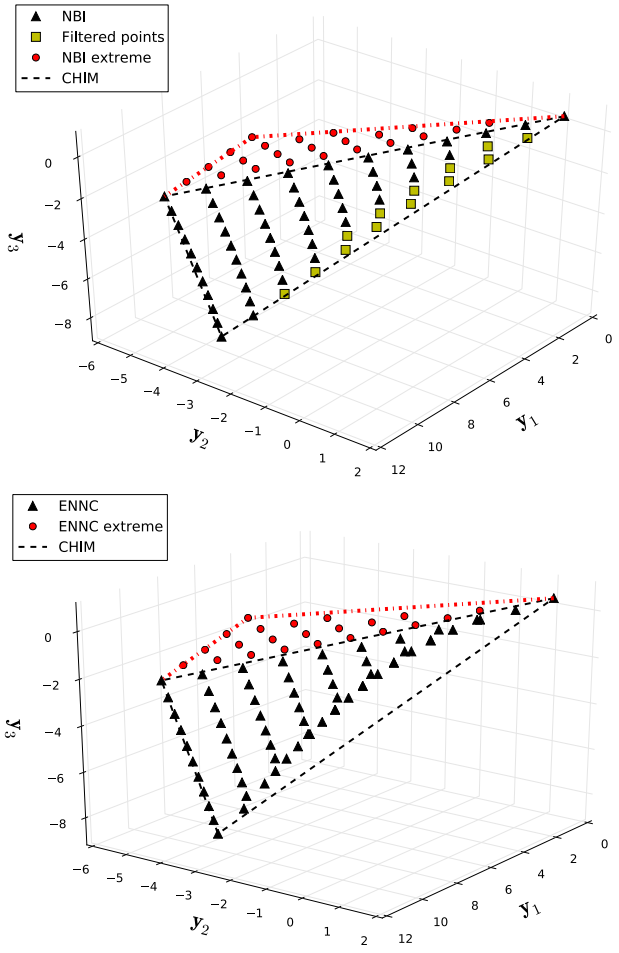

Figure 14: Extended Pareto set achieved with the NBI method (top) and extended Pareto set obtained with the ENNC method (bottom) for Case III.

575 independent variable Logist et al. (2012):

$$\frac{d}{dz}x_1(z) = \frac{\alpha}{v}(1-x_1)e^{\frac{\gamma x_2}{1+x_2}} \quad (51)$$

$$\frac{d}{dz}x_2(z) = \frac{\alpha\delta}{v}(1-x_1)e^{\frac{\gamma x_2}{1+x_2}} + \frac{\beta}{v}(u-x_2) \quad (52)$$

with initial conditions:

$$x_1(0) = 0 \text{ and } x_2(0) = 0 \quad (53)$$

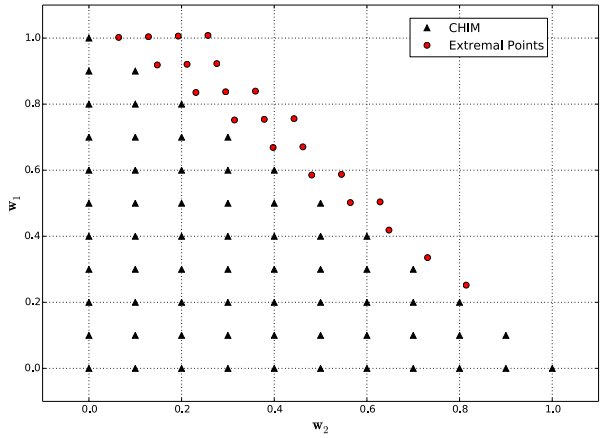

Figure 15: Scalarization parameter space for Case III. Only one *extreme* region was detected and discretized for this case study. The third scalarization parameter can be calculated as the complement to one of the sum of the other two.

and constraints:

$$\frac{T_{\min} - T_{\text{in}}}{T_{\text{in}}} \leq x_2(z) \leq \frac{T_{\max} - T_{\text{in}}}{T_{\text{in}}} \tag{54}$$

$$\frac{T_{\text{w,min}} - T_{\text{in}}}{T_{\text{in}}} \leq u(z) \leq \frac{T_{\text{w,max}} - T_{\text{in}}}{T_{\text{in}}} \tag{55}$$

$$L_{\min} \leq L \leq L_{\max} \tag{56}$$

$$0.85 \leq x_1(L)\ . \tag{57}$$

The states are the dimensionless reactant concentration $x_1 = (C_{\text{in}} - C)/C_{\text{in}}$ and reactor temperature $x_2 = (T - T_{\text{in}})/T_{\text{in}}$. Here, T_{in} and C_{in} are the temperature and the reactant concentration of the feed stream. The control $u = (T_{\text{w}} - T_{\text{in}})/T_{\text{in}}$ is a dimensionless version of the jacket temperature T_{w}. For constructive reasons, bounds are imposed on the reactor and jacket temperatures, as well as on the reactor length (constraints (54) to (56)). For economic reasons, a lower limit of 0.85 is applied on the conversion (constraint (57)).

The aim is to derive an optimal profile along the reactor for the jacket temperature profile $u(z)$. The three objectives considered are similar to the

conflicting ones treated in Logist et al. (2009): (i) maximizing the conversion, which is related to minimizing the reactant concentration at the outlet:

$$J_1 = 100 C_{\text{in}}(1 - x_1(L)) \tag{58}$$

(ii) maximizing the net heat transfer between the reactor and its jacket, where heat transferred from the reactor to the jacket is assumed to be a profit:

$$J_2 = 1000 \int_0^L \frac{\beta}{L}(u(z) - x_2(z))dz \tag{59}$$

and (iii) minimizing the installation cost, which is related to the reactor length:

$$J_3 = L. \tag{60}$$

For parameter values, the reader is referred to Logist et al. (2009).

This case study represents an example of MOOCP. Hence, every SOOP in which the multi-objective problem is discretized will be an optimal control problem. To solve each optimal control problem numerically, an orthogonal collocation technique with a piecewise constant control discretization of 50 uniform pieces and a state discretization with Lagrange third order polynomials is used. The arising large-scale NLP accounts for 652 optimization variables of which 52 are degrees of freedom. Additionally, the problem is subjected to 600 equality and 1318 inequality constraints. In particular, the 52 degrees of freedom are: 50 piecewise constant control actions, the additional variable introduced by the NBI method and the *free* end point variable. For the ENNC method only 51 degrees of freedom are present since no additional variable is introduced.

Figure 16 illustrates all the *external*, *outer* and *horizon* points obtained by applying the IGE procedure to this case study. In particular, all three *extreme* regions have different sizes. Hence, a different number of points (i.e., 22, 8 and 15 points) will be used to discretize them. Also for this case study the parameter p is set to 11. Hence, according to Eq. (36) 66 points are evenly distributed over the CHIM. The total amount of points used for the discretization

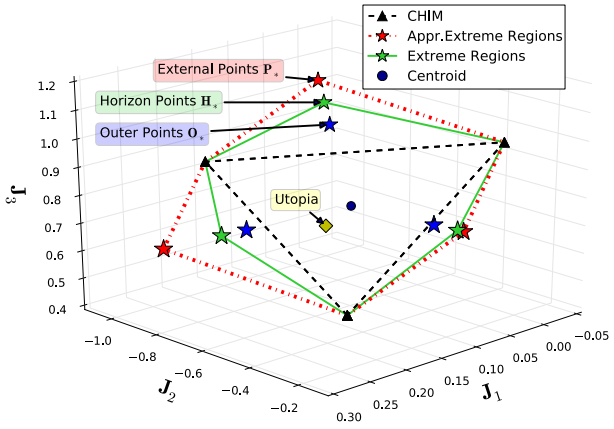

Figure 16: All geometric elements obtained when the proposed IGE proposed is applied to Case IV. Note the different sizes of each detected *extreme* region.

of the CHIMH is 111. The scalarization parameter space is reported in the top graph of Figure 17 by means of the 111 points in which it is discretized. In line with the previous example the third scalarization parameter can be calculated as the complement to one of the sum of the others.

The bottom graph in Figure 17 depicts the generated Pareto front for the ENNC method. As for Cases I and II, a similar result was achieved with the NBI method. The different trade-offs can easily be recognized. Higher reactor temperatures increase conversion but also increase the net energy cost. Longer reactors increase productivity but also installation cost. Longer tubes are able to recover on average more energy, however, at the expense of larger investment costs. The computational time needed for the NBI method to produce all the 111 points is 64.55 s, while the ENNC method required 44.28 s in total. An overview of the required CPU times is reported in Table 2.

Since every point on the Pareto set reported in Figure 17 represents an optimal control problem solution, a small set of solutions is selected and the

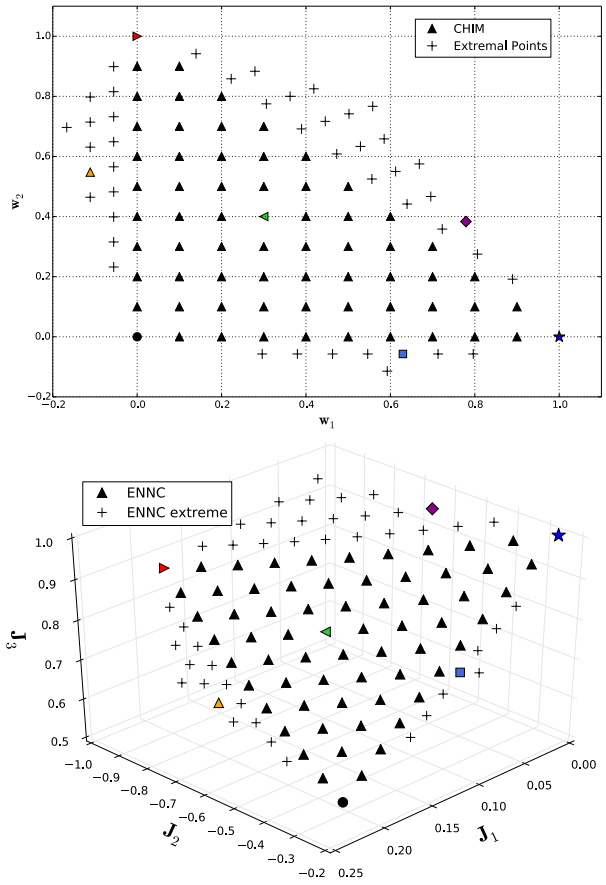

Figure 17: Scalarization parameter space for Case IV (top) and extended exploration of the criterion space with the ENNC method (bottom). A subset of solutions is selected and reported in both graphs. Hence, for each selected solution the set of scalarization parameters is identified. Moreover, the control profile corresponding to each selected solution is reported in Figure 18.

corresponding control profiles are shown in order to appreciate the different control actions. The control action profiles, obtained from the solution of the anchor points and the selected subproblems in both graphs in Figures 17, are reported in Figure 18. Again, it is possible to distinguish the trade-offs among the objectives: (i) a longer reactor enables a better conversion and more energy to be extracted and (ii) if the jacket temperature is lowered more energy is

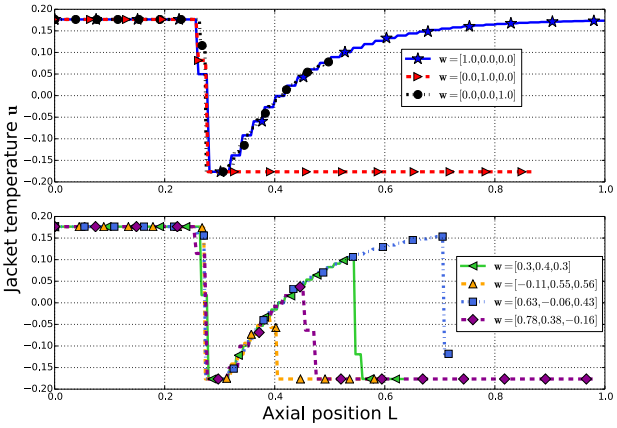

Figure 18: Control profiles obtained from the solution of the selected subproblems in Figure 17. The top graph reports the results for the anchor points, while the bottom one for the selected points reported in both graphs in Figures 17.

extracted causing a worse conversion.

5.5. Case V: Multi-Objective Optimal Control of a Batch Reactor

The fifth and last case study reported here is the the Williams-Otto batch reactor. Inside the batch reactor the following reaction scheme take place: $A + B \rightarrow C$, $C + B \rightarrow P + E$ and $P + C \rightarrow G$. From these compounds, A is initially present in the reactor and B is fed. The products P and E are useful products, whereas product G is an undesired by-product. The reactor model

can be expressed as follows:

$$\frac{\mathrm{d}}{\mathrm{d}t}x_A(t) = -\frac{x_A u_1}{V} - (k_1\eta_1 x_A x_B) * 1000, \tag{61}$$

$$\frac{\mathrm{d}}{\mathrm{d}t}x_B(t) = \frac{(1-x_B)u_1}{V} - (k_1\eta_1 x_A x_B - k_2\eta_2 x_B x_C) * 1000, \tag{62}$$

$$\frac{\mathrm{d}}{\mathrm{d}t}x_C(t) = -\frac{x_C u_1}{V} + (k_7\eta_1 x_A x_B - k_3\eta_2 x_B x_C - k_6\eta_3 x_C x_P) * 1000, \tag{63}$$

$$\frac{\mathrm{d}}{\mathrm{d}t}x_P(t) = -\frac{x_P u_1}{V} + (k_2\eta_2 x_B x_C - k_4\eta_3 x_C x_P) * 1000, \tag{64}$$

$$\frac{\mathrm{d}}{\mathrm{d}t}x_E(t) = -\frac{x_E u_1}{V} + (k_3\eta_2 x_B x_C) * 1000, \tag{65}$$

$$\frac{\mathrm{d}}{\mathrm{d}t}x_G(t) = -\frac{x_G u_1}{V} - (k_5\eta_3 x_C x_P) * 1000, \tag{66}$$

$$\begin{aligned}\frac{\mathrm{d}}{\mathrm{d}t}T(t) = {} & \frac{(T_\mathrm{F}-T)u_1}{V} + (k_8\eta_1 x_A x_B + k_9\eta_2 x_B x_C) * 1000 \\ & + (k_{10}\eta_3 x_C x_P - l_1(T - 1000u_2)) * 1000,\end{aligned} \tag{67}$$

$$\frac{\mathrm{d}}{\mathrm{d}t}V(t) = u_1, \tag{68}$$

where the states $x_i(t)$ for $i = A,\ B,\ C,\ P,\ E,\ G$ are the reactants and products concentrations, $T(t)$ represents the reactor temperature and $V(t)$ indicates the reaction liquid volume. The reactions can be controlled by adjusting the feed rate of reactant B, $u_1(t)$, and the cooling jacket temperature, $u_2(t)$. All the model parameters, their values, the initial condition and additional constraints are reported in literature (Hannemann & Marquardt (2010); Logist et al. (2012)).

In this work the following objective functions are considered: J_1 the maximisation of product P , J_2 the minimisation of by-product G and J_3 the minimization of batch time:

$$J_1 = -x_E(t_\mathrm{f})V(t_\mathrm{f}), \quad \text{with: } J_1 \geq 0.6 \tag{69}$$

$$J_2 = x_G(t_\mathrm{f})V(t_\mathrm{f}), \quad \text{with: } J_2 \leq 0.8 \tag{70}$$

$$J_3 = t_\mathrm{f}, \quad \text{with: } 0.5 \leq J_3 \leq 1.0. \tag{71}$$

$$\tag{72}$$

The limits on the objective functions are introduced in this work. Addi-

tionally, here the dynamic model is normalized by scaling the the independent variable representing the batch time t between 0 and 1. As in the previous case study also here an orthogonal collocation technique with a piecewise constant control discretization of 50 uniform pieces and a state discretization with Lagrange third order polynomials is used. The arising large-scale NLP accounts for 1702 optimization variables of which 102 are degrees of freedom. Additionally, the problem is subjected to 12500 equality and 155 inequality constraints. In particular, the 102 degrees of freedom are: 50 piecewise constant control actions each for the two control variable u_1 and u_2, the additional variable introduced by the NBI method and the *free* end time t_f. For the ENNC method only 51 degrees of freedom are present since no additional variable is introduced.

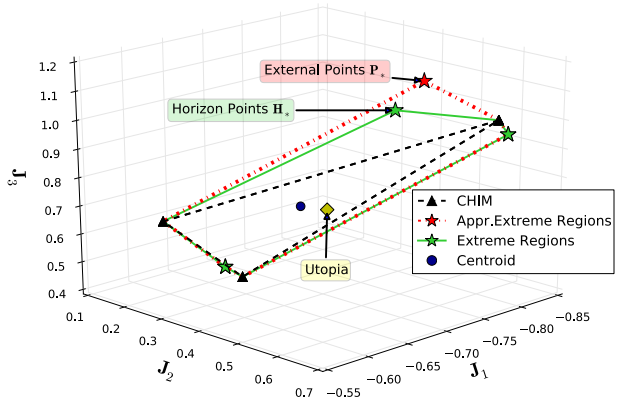

Figure 19: All geometric elements obtained when the proposed IGE proposed is applied to Case V. Note the different sizes of each detected *extreme* region.

Figure 19 illustrates the application of the IGE procedure to this case study. In particular, also for this case the three *extreme* regions have different sizes. In particular, one region collapses on the border of the CHIM, hence no additional point is generated in that region. For the other two *extreme* regions 16 and 10 points are used. For this case study the parameter p is set to 8. Hence, according to Eq. (36) 36 points are evenly distributed over the CHIM. The

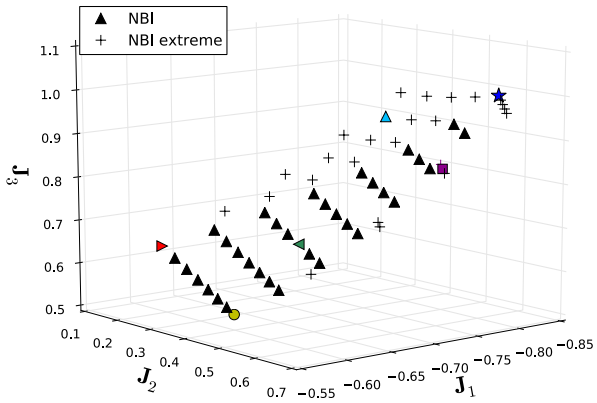

Figure 20: Extended exploration of the criterion space with the NBI method for Case V. A subset of solutions is selected in the bottom graphs. For each selected solution the set of scalarization parameters is identified. Moreover, the control profile corresponding to each selected solution is reported in Figure 21.

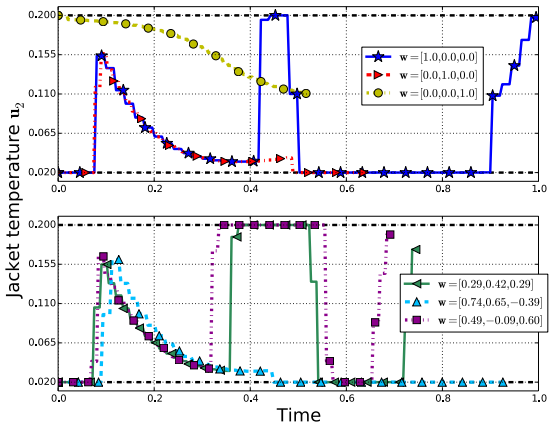

Figure 21: Control profiles obtained from the solution of the selected subproblems in Figure 20. The top graph reports the results for the anchor points, while the bottom one for some intermediate solutions.

total amount of points used for the discretization of the CHIMH is 62. The scalarization parameter space is not reported for this case study for the sake of

brevity, however all consideration previously illustrated hold for this case as well.

The graph in Figure 20 depicts the generated Pareto front for the NBI method. As for Cases I and II, a similar result was achieved with the ENNC method. It is possible to clearly identify the arising trade-offs between the considered objective functions. Longer batch time allow for more product P to be generated however also the amount of by-product G increases. Higher jacket fluid temperature, i.e. the presence of the max arc, after the constrained arc (around $t = 0.4$) boost the production of product P, while the absence of the max arc generate the opposite effect limiting the production of G. Finally shorter batch time allows for more batches to be run during the day, hence, possibly increasing the variety of products produced between different batches.The computational time needed for the NBI method to produce the 62 points is 333.83 s, while the ENNC method required 206.35 s in total. An overview of the required CPU times is reported in Table 2.

As for the previous optimal control case study a set of optimal solutions is selected and the relative control profiles for u_2 are depicted. The control action profiles, obtained from the solution of the anchor points and the selected subproblems in Figure20, are reported in Figure 21.

5.6. Results overview

All numerical optimization problems are solved with an in-house developed software. The software is based on the open source package for automatic differentiation CasADi Andersson et al. (2012) and exploits Ipopt Wächter & Biegler (2006) as interior point NLP solver. Since the optimization framework uses gradient based approaches, there are no guarantees that the global optimum will be reached unless the considered problem is convex. All problems are solved with a desktop computer featuring an Intel Core2 Quad, with four CPUs at 3.00 GHz each and 4 Gb of RAM. The IGE procedure proposed in this work was successfully applied to all case studies. In particular similar results to the

	p	m	p_{CHIM}	N_{ext} ($p_{ext,i}$)	p_{TOT}
Case I	12	3	78	3 (15/15/15)	123
Case II	10	4	220	4 (39/39/39/39)	376
Case III	11	3	66	1 (22)	88
Case IV	11	3	66	3 (22/8/15)	111
Case V	8	3	36	2 (16/10)	62

Table 1: Overview of the number of SOOPs formulated and solved for each case study.

ones obtained by Motta et al. (2012) are found for the Case I and II, while the obtained computation times are an order of magnitude lower. Motta et al. (2012) do not report any information on the hardware used in their work. However, since the hardware used in this work was acquired in September 2010, it is assumed that its computational power is comparable with the one used in by Motta et al. (2012). Additionally, the computation time for the IGE is in most of the cases less than 20 % of the total computation time. It is interesting to notice that the IGE procedure does not require additional computation effort when applied to the higher dimensional problem Case II. On the contrary, a significant computational burden is required for the IGE procedure for Case III. This is due to the non-convex shape of the feasible criteria space $\mathcal{J}$ for Case III. This can be seen by the high computational time required also for the ENNC method were the obtuse angle disappears due to the mapping of the vertices to a unit hyper-cube. The adopted set of case studies corroborates the generic applicability of the proposed IGE procedure. In particular, the possibility for interaction with the decision maker and the low computation time required makes the IGE particularly suitable for computationally demanding problems, such as optimal control problems.

6. Conclusions

This paper has introduced a novel procedure based on geometric considerations to interactively extend the explored region of the Pareto set for multi-

method	total time (s)/ per point (s)	IGE (s)	total time percentage (%)
Case I			
NBI	0.83 s / 0.0071 s	0.17 s	20.4%
ENNC	1.02 s / 0.0085 s	0.07 s	14.6%
Case II			
NBI	2.16 s / 0.0058	0.23 s	10.6%
ENNC	2.86 s / 0.0077 s	0.12 s	4.1%
Case III			
NBI	2.57 s / 0.029 s	1.73 s	67.3%
ENNC	1.94 s / 0.022 s	1.10 s	56.7%
Case IV			
NBI	64.55 s / 0.63 s	7.72 s	11.9%
ENNC	44.28 s / 0.40 s	2.85 s	6.4%
Case V			
NBI	333.83 s / 5.38 s	45.84 s	13.7%
ENNC	206.35 s / 3.33 s	26.51 s	12.8%

Table 2: Overview of the computational time needed to achieve the extended exploration of the criterion space.

objective optimization approaches such as ENNC/NBI. In particular the strategy was successfully applied to a series of case studies demonstrating its general applicability. Additionally, the procedure exhibits a low computational burden. This is particularly appealing for optimal control problems, since their solution can by itself become expensive from a computation point of view. Moreover, the procedure is applicable to higher dimensionality problems, i.e., more then three objectives. However, an effective visualization of results is not trivial. Finally, the procedure gives rise to a natural interactive approach for the exploration of the Pareto set according to the DM's preferences. This opens interesting scenarios for the development of tailored software to include active human interaction during the optimization procedure.

ACKNOWLEDGMENTS

Mattia Vallerio and Dominique Vercammen both have a Ph.D. grant of the Agency for Innovation through Science and Technology in Flanders (IWT). The research was supported by KUL: PFV/10/002 (OPTEC), the Flemish Government via FWO-projects: FWO-1518913N and FWO-G.0930.13 and the Belgian Federal Science Policy Office: IAP VII/19 (DYSCO).

References

Agrawal, N., Rangaiah, G., Ray, A., & Gupta, S. (2006). Multi-objective optimization of the operation of an industrial low-density polyethylene tubular reactor using genetic algorithm and its jumping gene adaptations. *Industrial and Engineering Chemistry Research*, *45*, 3182–3199.

Alvarez-Vázquez, L., García-Chan, N., Martínez, A., & Vázquez-Méndez, M. (2010). Multi-objective pareto-optimal control: an application to wastewater management. *Computational Optimization and Applications*, *46*, 135–157.

Andersson, J., Åkesson, J., & Diehl, M. (2012). CasADi – A symbolic package for automatic differentiation and optimal control. In *Recent Advances in Algorithmic Differentiation* (pp. 297–307). Springer Berlin Heidelberg volume 87.

Bhaskar, V., Gupta, S., & Ray, A. (2000). Applications of multi-objective optimization in chemical engineering. *Reviews in Chemical Engineering*, *16*, 1–54.

Biegler, L. (1984). Solution of dynamic optimization problems by successive quadratic programming and orthogonal collocation. *Computers and Chemical Engineering*, *8*, 243–248.

Biegler, L. (2007). An overview of simultaneous strategies for dynamic optimization. *Chemical Engineering and Processing: Process Intensification*, *46*, 1043–1053.

Bock, H., & Plitt, K. (1984). A multiple shooting algorithm for direct solution of optimal control problems. In *Proceedings of the 9th IFAC world congress, Budapest* (pp. 243–247). Pergamon Press.

Chaudhuri, S., & Deb, K. (2010). An interactive evolutionary multi-objective optimization and decision making procedure. *Applied Soft Computing*, *10*, 496 – 511.

Das, I., & Dennis, J. (1997). A closer look at drawbacks of minimizing weighted sums of objectives for Pareto set generation in multicriteria optimization problems. *Structural Optimization*, *14*, 63–69.

Das, I., & Dennis, J. (1998). Normal-Boundary Intersection: A new method for generating the Pareto surface in nonlinear multicriteria optimization problems. *SIAM Journal on Optimization*, *8*, 631–657.

Deb, K. (2001). *Multi-Objective Optimization Using Evolutionary Algorithms*. Chichester, London, UK: John Wiley.

Deb, K., & Jain, H. (2014). An evolutionary many-objective optimization algorithm using reference-point-based nondominated sorting approach, part i: Solving problems with box constraints. *Evolutionary Computation, IEEE Transactions on*, *18*, 577–601.

Deb, K., Mitra, K., Dewri, R., & Majumdar, S. (2004). Towards a better understanding of the epoxy-polymerization process using multi-objective evolutionary computation. *Chemical Engineering Science*, *59*, 4261 – 4277.

Du, Q., Faber, V., & Gunzburger, M. (1999). Centroidal voronoi tessellations: applications and algorithms. *SIAM Review*, *41*, 637–676.

Duran, M. A., & Grossmann, I. E. (1986). An outer-approximation algorithm for a class of mixed-integer nonlinear programs. *Mathematical Programming*, *36*, 307–339.

Eichfelder, G. (2008). *Adaptive Scalarization Methods in Multiobjective Optimization*. Vector Optimization. Springer.

Eichfelder, G. (2009a). An adaptive scalarization method in multiobjective optimization. *SIAM Journal on Optimization*, *19*, 1694–1718.

Eichfelder, G. (2009b). Scalarizations for adaptively solving multi-objective optimization problems. *Computational Optimization and Applications*, *44*, 249–273.

Fletcher, R., & Leyffer, S. (1994). Solving mixed integer nonlinear programs by outer approximation. *Mathematical Programming*, *66*, 327–349.

Gong, D., Ji, X., Sun, J., & Sun, X. (2014). Interactive evolutionary algorithms with decision-makers preferences for solving interval multi-objective optimization problems. *Neurocomputing*, *137*, 241 – 251.

Haimes, Y., Lasdon, L., & Wismer, D. (1971). On a bicriterion formulation of the problems of integrated system identification and system optimization. *IEEE Transactions on Systems, Man, and Cybernetics*, *SMC-1*, 296–297.

Hakanen, J., Miettinen, K., Mäkelä, M., & Manninen, J. (2005). On interactive multiobjective optimization with NIMBUS in chemical process design. *Journal of Multicriteria Decision Analysis*, *13*, 125–134.

Hannemann, R., & Marquardt, W. (2010). Continuous and discrete adjoints for the hessian of the lagrangian in shooting algorithms for dynamic optimization. *SIAM Journal on Scientific Computing*, *31*, 4675–4695.

Hettenhausen, J., Lewis, A., & Kipouros, T. (2014). A web-based system for visualisation-driven interactive multi-objective optimisation. *Procedia Computer Science*, *29*, 1915–1925. 2014 International Conference on Computational Science.

Jahn, J. (1984). Scalarization in vector optimization. *Mathematical Programming*, *29*, 203–218.

Jaszkiewicz, A., & Słowinski, R. (1999). The 'Light Beam Search' approach an overview of methodology and applications. *European Journal of Operational Research*, *113*, 300–314.

Kim, I., & de Weck, O. (2006). Adaptive weighted sum method for multiobjective optimization: a new method for Pareto front generation. *Structural and Multidisciplinary Optimization*, *31*, 105–116.

Kollat, J. B., & Reed, P. (2007). A framework for visually interactive decision-making and design using evolutionary multi-objective optimization (video). *Environmental Modelling & Software*, *22*, 1691 – 1704.

Konak, A., Coit, D., & Smith, A. (2006). Multi-objective optimization using genetic algorithms: a tutorial. *Reliability Engineering and System Safety*, *91*, 992–1007.

Leineweber, D., Bauer, I., Bock, H., & Schlöder, J. (2003). An efficient multiple shooting based reduced SQP strategy for large-scale dynamic process optimization. Part I: theoretical aspects. *Computers and Chemical Engineering*, *27*, 157–166.

Logist, F., Houska, B., Diehl, M., & Van Impe, J. (2010a). Fast pareto set generation for nonlinear optimal control problems with multiple objectives. *Structural and Multidisciplinary Optimization*, *42*, 591–603.

Logist, F., Houska, B., Diehl, M., & Van Impe, J. (2011). Robust multi-objective optimal control of uncertain (bio)chemical processes. *Chemical Engineering Science*, *66*, 4670 – 4682.

Logist, F., Sager, S., Kirches, C., & Van Impe, J. (2010b). Efficient multiple objective optimal control of dynamic systems with integer controls. *Journal of Process Control*, *20*, 810–822.

Logist, F., Vallerio, M., Houska, B., Diehl, M., & Van Impe, J. (2012). Multi-objective optimal control of chemical processes using ACADO toolkit. *Computers and Chemical Engineering*, *37*, 191–199.

Logist, F., Van Erdeghem, P., Smets, I., & Van Impe, J. (2009). Optimal design of dispersive tubular reactors at steady-state using optimal control theory. *Journal of Process Control*, *19*, 1191–1198.

Logist, F., & Van Impe, J. (2012). Novel insights for multi-objective optimisation in engineering using normal boundary intersection and (enhanced) normalised normal constraint. *Structural and Multidisciplinary Optimization*, *45*, 417–431.

Marler, R., & Arora, J. (2004). Survey of multi-objective optimization methods for engineering. *Structural and Multidisciplinary Optimization*, *26*, 369–395.

Messac, A., & Mattson, C. (2004). Normal constraint method with guarantee of even representation of complete Pareto frontier. *AIAA Journal*, *42*, 2101–2111.

Miettinen, K. (1999). *Nonlinear multiobjective optimization*. Boston: Kluwer Academic Publishers.

Miettinen, K., & Mäkelä, M. (1995). Interactive bundle-based method for non-differentiable multiobjeective optimization: NIMBUS. *Optimization*, *34*, 231–246.

Motta, R. d. S., Afonso, S. M. B., & Lyra, P. R. M. (2012). A modified NBI and NC method for the solution of N-multi-objective optimization problems. *Structural and Multidisciplinary Optimization*, *46*, 239–259.

Mueller-Gritschneder, D., Graeb, H., & Schlichtmann, U. (2009). A successive approach to compute the bounded pareto front of practical multiobjective optimization problems. *SIAM Journal on Optimization*, *20*, 915–934.

Ojalehto, V., Miettinen, K., & Laukkanen, T. (2014). Implementation aspects of interactive multiobjective optimization for modeling environments: the case of GAMS-NIMBUS. *Computational Optimization and Applications*, (pp. 1–23).

Pascoletti, A., & Serafini, P. (1984). Scalarizing vector optimization problems. *Journal of Optimization Theory and Applications*, *42*, 499–524.

Sanchis, J., Martinez, M., Blasco, X., & Salcedo, J. (2008). A new perspective on multiobjective optimization by enhanced normalized normal constraint method. *Structural and Multidisciplinary Optimization*, *36*, 537–546.

Sarkar, D., & Modak, J. (2004). Optimization of fed-batch bioreactors using genetic algorithm: multiple control variables. *Computers & Chemical Engineering*, *28*, 789–798.

Sinha, A., Korhonen, P., Wallenius, J., & Deb, K. (2014). An interactive evolutionary multi-objective optimization algorithm with a limited number of decision maker calls. *European Journal of Operational Research*, *233*, 674 – 688.

Steuer, R. E., & Choo, E. (1983). An interactive weighted tchebycheff procedure for multiple objective programming. *Mathematical Programming*, *26*, 326–344.

Vallerio, M., Van Impe, J., & Logist, F. (2014). Tuning of nmpc controllers via multi-objective optimisation. *Computers & Chemical Engineering*, *61*, 38–50.

Wächter, A., & Biegler, L. (2006). On the implementation of a primal-dual interior point filter line search algorithm for large-scale nonlinear programming. *Mathematical Programming*, *106*, 25–27.

Yalçma Kaya, C., & Maurer, H. (2014). A numerical method for nonconvex multi-objective optimal control problems. *Computational Optimization and Applications*, *57*, 685–702.